ACME

ARCHIVES
OF CIVIL AND MECHANICAL
ENGINEERING

Quarterly
Vol. I, No. 1

WROCŁAW 2001

ARCHIVES
OF CIVIL AND MECHANICAL
ENGINEERING

Contents

Spis treści

Foreword

The aim of this journal is to present the latest achievements in civil and mechanical engineering. We intend to publish papers written not only by Polish scientists, but also by scientists from foreign centres. This journal offers them all an opportunity to exchange ideas and experience.

Many-year common activities of civil engineers and mechanical engineers under the auspices of Professor Edmund Małachowicz, the President of the Polish Academy of Sciences – Wrocław Branch, the Committee of Civil and Mechanical Engineering PAS – Wrocław Branch and the deans of the Civil Engineering Faculty and the Mechanical Engineering Faculty of the Wrocław University of Technology have given us an idea of publishing this journal. The idea has also been supported by Professor Andrzej Mulak, the President of the Wrocław University of Technology.

Numerous problems in the two scientific fields are closely related. The affinities are so strong that often it is hard to decide whether a given paper deals with civil or mechanical engineering. It is not only the main branches of knowledge such as applied mathematics, physics, chemistry and informatics, but first of all the basic fields of technology such as mechanics, theory of structures, materials science, computational methods for design, and manufacturing processes that can contribute to the solution of the engineering problems. Therefore, the scope of the journal cannot be too narrow.

Archives of Civil and Mechanical Engineering (ACME) publishes both theoretical and experimental papers which explore or exploit new ideas and techniques in the following areas: structural engineering (structures, machines and mechanical systems), mechanics of materials (elasticity, plasticity, rheology, fatigue, fracture mechanics), materials science (metals, composites, ceramics, plastics, wood, concrete, etc., their structure and properties, methods of evaluation), manufacturing engineering (process design, simulation, diagnostics, maintenance, durability, reliability). In addition to research papers, the Editorial Board welcome: state-of-the-art reviews of specialized topics, letters to the Editor for quick publication, brief work-in-progress reports, brief accounts of completed doctoral thesis (one page is maximum), and bibliographical note on habilitation theses (maximum 250 words). All papers are subject to a referee procedure, except for letters, work-in-progress reports and doctoral and habilitation theses, which are briefly reviewed by the Editorial Board.

The papers submitted have to be unpublished works and should not be considered for publication elsewhere.

The Editorial Board would be grateful for all comments on the idea of the journal.

Professor Jerzy Gronostajski,
Professor Jan Kmita

Principles of modelling of the surface machining by high-pressure abrasive-water jet using genetic algorithm

J. BORKOWSKI, P. BORKOWSKI, A. KOWALEWSKI

Technical University of Koszalin, Raclawicka 15–17, 75-620 Koszalin

The genetic algorithm presented in the paper was developed to search for favourable conditions of cleaning by means of the high-pressure abrasive-water jet. Due to application of specific numerical procedures the linear mono-parametric models of the surface machining process were developed. On the basis of process parameters stored in as the input data, the genetic algorithm enabled us to determine the optimal process parameters for surface treatment of corroded steel plates implemented using the high-pressure abrasive-water jet.

Keywords: *surface machining, modelling, high-pressure abrasive-water jet, genetic algorithm*

1. Introduction

The objective of this work was to generate the genetic algorithm for optimization of surface processing conditions using the high-pressure abrasive-water jet. Various numerical techniques were used to produce a mathematical model based on relations between the process parameters. An analysis of essential parameters affecting the effectiveness and the results of studies into such surface treatment sufficed to develop such a model. The numerical procedure obtained, which allows the optimal process parameters to be selected, gives consideration of constraints and information available from experimental studies [4, 7].

The results of investigations of the removal of corrosive tarnish [6] were used for implementation of this task. The experimental studies were based on such process parameters as: the water pressure and water consumption [7], the feed and the distance between the nozzle outlet and the work surface [6], the abrasive granularity [5] and the abrasive consumption [4] and their effect on the process productivity [6, 7].

The application of the artificial neural network enabled us to evaluate correlation between input and output variables [8]. The artificial neural network applied here was designed in such a way that the above input quantities affected its output parameter, i.e. the process productivity. The procedure applied resulted in finding such artificial neural network that enabled us to achieve the fitness function, whereas the optimal process parameters were determined by means of the genetic algorithms. Water jet cleaning is characterized by a large number of variables, representing mechanical and geometrical

properties of the surface, properties of the deposit, deposit distribution and its adhesion, geometry and dynamics of the water jet, properties of the processing medium, etc. [10].

The method, the type and the extensiveness of corrosion and the parameters of its cleaning are very complicated and information about them is rather limited. Various artificial intelligence techniques enable us to achieve an immediate access to the control of the values of process parameters in a way allowing one to obtain the satisfactory results of surfacing [1].

This is a branch of science which has aroused a growing interest in scientific workers quite lately. However, within the compass of several dozen years a lot of works have appeared which demonstrate the application of the artificial neural network for solving the complex problems. Recently this procedure has been applied to the optimization of jet-based material cleaning [2, 3].

The present paper discusses the issues essential for correct modelling of the process of surface-corrosion removal carried out using a more complicated tool, i.e. the high-pressure abrasive-water jet. The process parameters of such a treatment were optimized using the genetic algorithms.

2. Introduction to artificial neuron network and genetic algorithms

An artificial neuron network consists of many interconnected identical elementary processing units or neurons whose architecture is inspired by the structure of the cerebral cortex of the brain. A neuron is a simple processing unit, which consists of two parts. The first part simply sums up all the weighted inputs from other neurons, while the second part modifies this aggregated signal by applying an activation function to it. The input signals $x_1, x_2, x_3, \ldots, x_n$ are sent to processing units through the network's connections [8]. The connections between neurons in a network are assigned the so-called weights (w_n), which modify input signal, making it either positive or negative, which corresponds to acceleration or inhibition of the signal in a biological neuron [9].

The genetic algorithms are used for solving the problems in a way simulating certain processes taking place in nature – more exactly the rule of survival of the fittest. As one can imagine, the evolution is the algorithm optimizing constantly a certain function – a fitness value. In nature, the generation of species is closely associated with their best adaptation to the ecosystem and in a similar way the person that solves the problem is searching for possible optimal solutions. Nature still does not create ideal species and similarly the genetic algorithms are used for searching only approximated results. However, such methods are extremely useful in practice. Facing up the difficult problem (i.e. which would give the exact solution but after reasonable time of processing) we usually accept the optimum solution, which does not differ much from the real one [11].

3. Neural network model of corrosive-tarnish removal process

In order to obtain an experimental data base required to actuate and train the artificial neuron network, the studies [4–7] of the conditions of corrosive-tarnish abrasive-water jet removal were carried out. The experiments were performed using the high-pressure spray gun, Type HP 750-2, produced by WOMA and equipped with a sprinkler with a multioutlet concentric nozzle. A hydro-monitor driven by an electric motor of a power of 94 kW, which generated the water jet at the pressure of 75 MPa, was also applied. Owing to that the database was generated, where 352 cases were isolated as useful for adequate selection and training of the neuron network. Artificial neuron networks allowed us to evaluate the correlation between the input and the output variables.

On the basis of the networks tested and after comparing their properties with the parameters of the process of corrosive tarnish removal, the linear artificial neuron network was applied. The network was trained by the pseudo-inversion, or the least-squares linear optimization method. The network trained through generation of its weights was applied to the genetic algorithm for the final optimization of the surface-treatment process carried out by the use of the high-pressure abrasive-water jet.

Making use of the data base obtained in the experimental studies, the process parameters were assumed and aliased with input and output neurons. Thus, among the input quantities x_1 determines the water pressure within the range of 20–30 MPa, x_2 – the water consumption of 25–40 dm^3/min, x_3 – the feed of 250–400 mm/min, x_4 – the jet length of 0.8–1.2 m, x_5 – the abrasive granularity of 0.2–1.2 mm, x_6 – the abrasive consumption of 4–10 kg/m^2. On the other hand, the only output quantity was y which determined the process productivity of 10–15 m^2/h. The relations obtained between the output parameter and the respective input parameters being linear in general are presented in Figures 1–3. However, in some cases the dependence of the input parameters on the process productivity is not always linear, forming a network of answers.
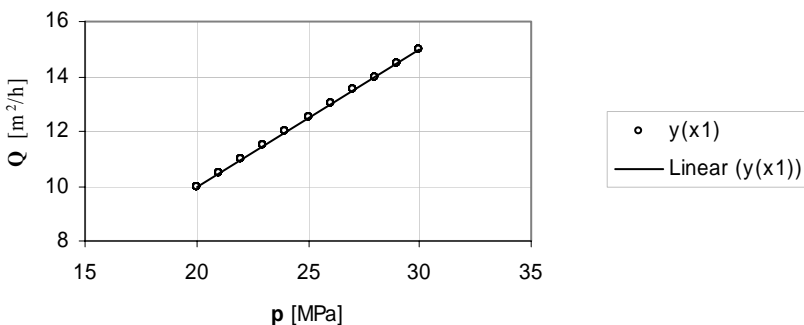
Fig. 1. The influence of water pressure on process productivity
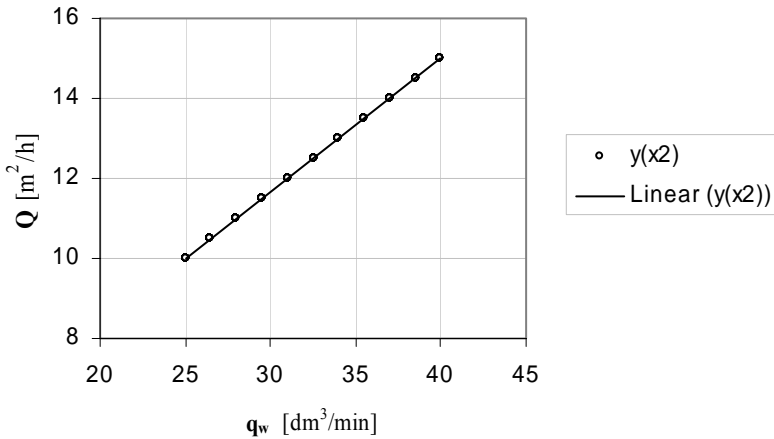
Fig. 2. The influence of water consumption on process productivity
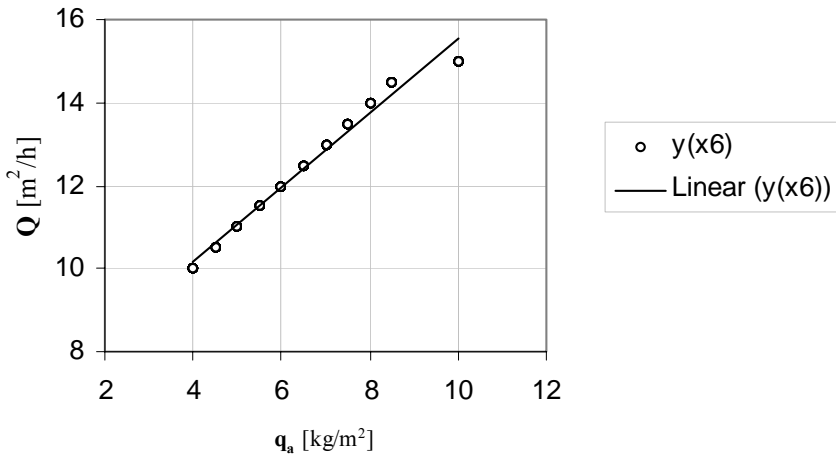
Fig. 3. The influence of abrasive consumption on process productivity

While searching for the best artificial neural network of a few thousands of neural networks tested in this process, the most advantages results gave the network of a linear structure. Only in few cases one could applied all parameters as input neurons for training. The idea of training the network with the teacher was selected. The diagram of the network applied is presented in Figure 4. In this type of training, the teacher, while asking the questions, prompts the answers, and in this case the answer is the target value of the network output.
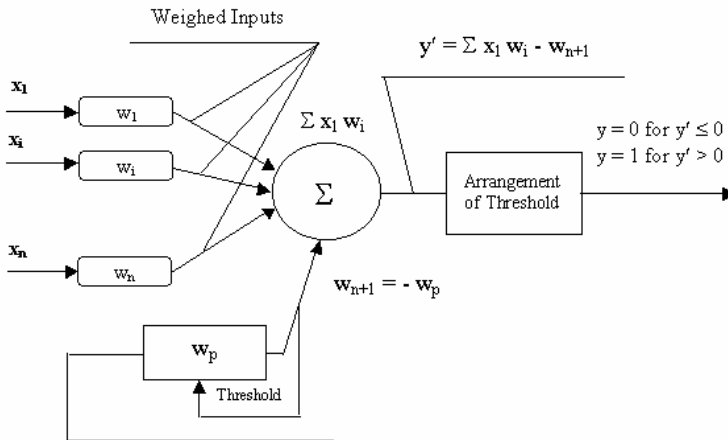
Fig. 4. Schema of the neural network applied

Among the experimental database three groups of data were isolated: a set of a training data (176 cases), a set of a validation data (88) or data checking the correctness of the network training and a testing set (88), which is presented in Figure 5.

Fig. 5. Example sheet of Statistica Neural Network

The network was trained using the PI-pseudo-inversion algorithm, or the linear optimization of the least squares. It was assumed for practical reasons that the neural network will be trained in 100 epochs. The correctness of this assumption is confirmed by the graphs presented in Figure 6.
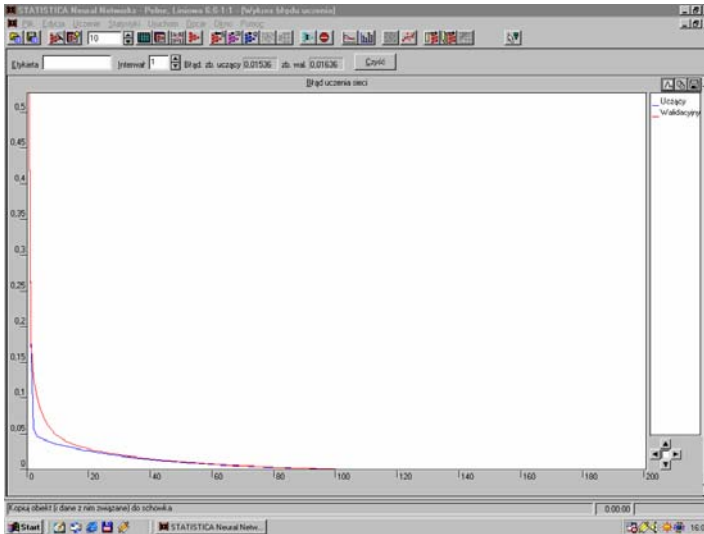
Fig. 6. Distribution of error values after consecutive epochs of the network training

On the basis of the weights obtained after training the artificial neural network, the target function was formulated and by the same token for further optimization of the relations between the respective process parameters. Values of the weights attached to the respective process parameters are presented in the Table.

Table. Values of weights for respective input data

Thresholds value	–0.1168
x_1 – water pressure	–0.6277
x_2 – water consumption	0.571533
x_3 – feed	–0.8201
x_4 – jet length	0.239441
x_5 – abrasive granularity	0.270447
x_6 – abrasive consumption	0.898132

4. Preparation of chromosome representation

A phenotype of the genetic algorithm comprising seven parameters was used for the task consisting in optimization of the fitness function. They come under the water pressure, the water consumption, the head feed, the distance between the nozzle outlet

and the surface being processed, the abrasive granularity, the abrasive consumption and the process productivity.

The parameters of the process that consisted in removal of corrosive tarnish were optimized by the genetic algorithm. Hence, making use of the experiments performed earlier we deal with the following values: the pressure of 20–30 MPa, the water consumption of 25–40 dm^3/min, the head feed of 250–400 mm/min, the distance between the nozzle outlet and the work surface of 0.8–1.2 m, the abrasive granularity of 0.2–1.2 mm, the abrasive consumption of 4–10 kg/m^2, the process productivity of 10–15 m^2/h.

A chromosome in the form of a binary vector was used for representation of a variable value of set parameters. A length of this vector depended on a required accuracy of the individuals from the respective intervals which, for example, were accepted to the second decimal place.

Thus, for the initial water pressure an interval value a was 20, and an interval length, or a domain of variation b is equal to 10. According to a required accuracy, an interval 20–30 was divided into at least 1000 equal subintervals. This results from multiplication of an interval length b by a numeral 100 determining an accuracy of individuals (the second decimal place). This means that the binary vector (chromosome) must include 10 bits (genes), because:

$$512 = 2^9 < 1000 \leq 2^{10} = 1024.$$

Therefore transformation of a binary string in the form of $<b_9 \, b_8...b_0>$ into a real number from the range of 20–30 can be carried out in two steps:
- transformation of a binary string

$$\left(< b_9 b_8...b_0 > \right)_2 = \left(\sum_{i=0}^{9} b_i 2^i \right)_{10} = x', \tag{1}$$

- calculation of a respective real number x:

$$x = \frac{a + bx'}{(2^{10} - 1)}, \tag{2}$$

where:
a – origin of an interval,
b – domain of variation (length of an interval).

Therefore for the parameter x to be studied:

$$x = \frac{20 + 10x'}{(2^{10} - 1)}.$$

For example, a chromosome in the form (1001110011) represents a number 26.13, because:

$$x' = (1001110011)_2 = 1 \cdot 2^0 + 1 \cdot 2^1 + 0 \cdot 2^2 + 0 \cdot 2^3 + 1 \cdot 2^4 + 1 \cdot 2^5 + 1 \cdot 2^6 + 0 \cdot 2^7 + 0 \cdot 2^8 + 1 \cdot 2^9 = 627,$$

$$x = 20 + 627 \cdot 10 / 1023 = 26.13.$$

To establish the bit representation for the next consecutive parameter we use the same procedure. Therefore for each of them we have:
• For the water consumption of 25–40 the required accuracy is to the second decimal place, or $a = 25$, $b = 15$. The interval is to be divided into 1500 equal subintervals, i.e. a binary vector must have 11 bits:
$\{1024 = 2^{10} < 1500 \le 2^{11} = 2048\}$
and will take the form of $<b_{10} \, b_9...b_0>$.
• For the feed of 250–400: $a = 250$, $b = 150$.
$\{8192 = 2^{13} < 15000 \le 2^{14} = 16384\}$.
A chromosome in this case will take the form of $<b_{13} \, b_{12}...b_0>$.
• For the jet length of 0.8–1.2: $a = 0.8$, $b = 0.4$.
$\{32 = 2^5 < 40 \le 2^6 = 64\}$.
A binary vector is $<b_5 \, b_4...b_0>$.
• For the abrasive granularity of 0.2–1.2: $a = 0.2$, $b = 1.0$.
$\{64 = 2^6 < 100 \le 2^7 = 128\}$.
A binary vector is $<b_6 \, b_5...b_0>$.
• For the abrasive consumption of 4–10: $a = 4$, $b = 6$.
$\{512 = 2^9 < 600 \le 2^{10} = 1024\}$.
A binary vector is $<b_9 \, b_8...b_0>$.
• For the process productivity of 10–15: $a = 10$, $b = 5$.
$\{256 = 2^8 < 500 \le 2^9 = 512\}$.
A binary vector is $<b_8 \, b_7...b_0>$.
The presented above chromosome representation is necessary to commence the task of optimization consisting in initiation or selection of initial population of chromosomes just represented by binary strings of specified length.

5. Optimization of corrosive-tarnish removal process

Through training the artificial neural network the data characterizing the fitness function was obtained, which in the further part was used for optimization of the process parameters. The model obtained was built of six process input variables and one output variable according to the above characteristics. In the same time, each

parameter was decided to divide into a number of bites determining a required accuracy. In this case, it will be to the second decimal point, and therefore:

• The binary representation of water pressure was expressed by a vector consisting of 10 bits, where a vector (0000000000) represented a value of 20 MPa, whereas (1111111111), a value of 30 MPa.
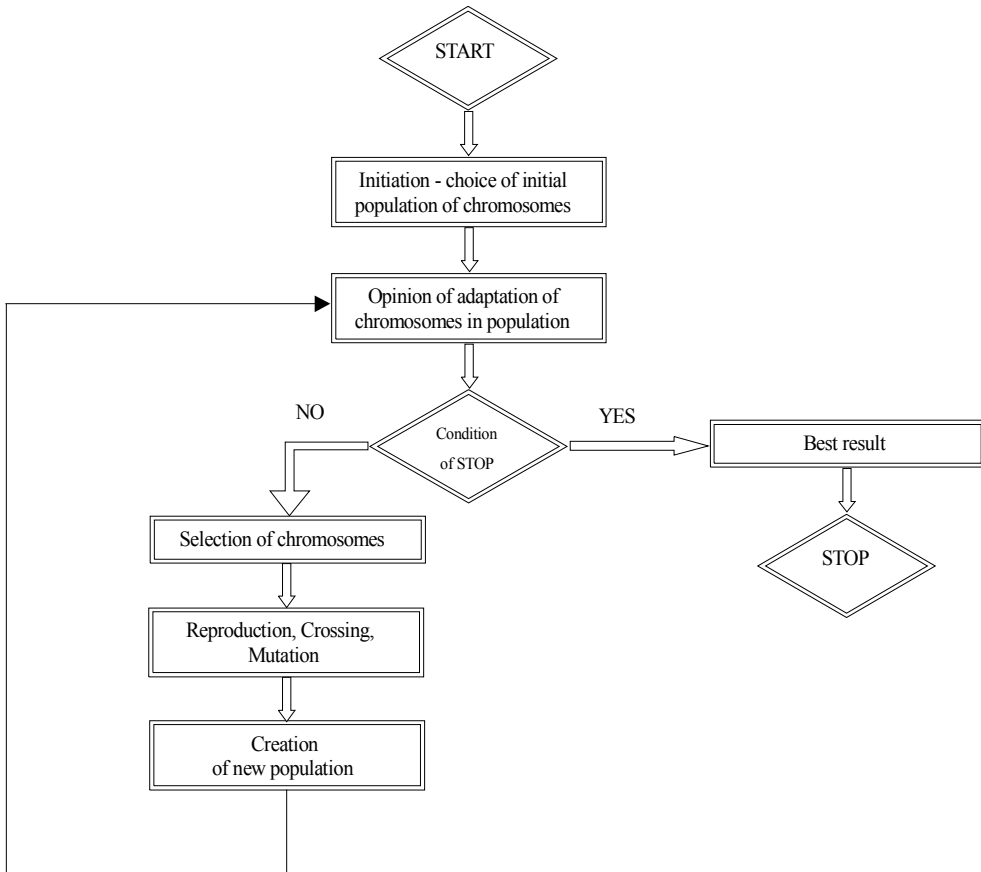
Fig. 7. Principle of operation of the genetic algorithm applied

• A binary vector of the water consumption consists of 11 bits (00000000000) equal to the value of 25 dm^3/min, whereas (11111111111), to the value of 40 dm^3/min.

• The feed is represented by fourteen-bit vector, hence (00000000000000) is equal to 250 mm/min, whereas (11111111111111), to 400 mm/min.

• To introduce a parameter determining the jet length, the representation consisting of six bits is required, where (000000) determines the value of 0.8 m, whereas (111111), the value of 1.2 m.

• The abrasive granularity is represented by a seven-bit vector (0000000) equal to 0.2 mm, whereas a vector (1111111), to 1.2 mm.

• A 10-bit representation was used to describe parameter of abrasive consumption, where a vector (0000000000) determines 4 kg/m^2, whereas (1111111111) is equal to 10 kg/m^2.

• And finally, the output parameter, i.e. the process productivity, is represented by 9 bits, the beginning of the interval under the study is equal to 10 m^2/h and in a bit representation it is in the form of (000000000), whereas a value of 15 m^2/h represents the form of (111111111).

The above bit representation of respective process parameters proves that the genetic algorithm searching for the optimum values operates on a chromosome consisting of 67 bits (10 + 11 + 14 + 6 + 7 + 10 + 9). Generation of such a bit vector determining the optimal values of process parameters was provided by the program being presented in a simplified form in Figure 7.

6. Optimization process results

The optimization process was carried out using the genetic algorithm enabling us to obtain the optimal values of the process parameters. After optimization of the process a 67-bit vector with the following values of respective parameters was obtained: 1110110101 10011111001 00111111000110 110110 0011000 1110111111 111111111, in which:

• water pressure in the form of a binary vector determines 1110110101 specified in MPa;
• water consumption determines 10011111001 specified in dm^3/min;
• feed determines 00111111000110 specified in mm/min;
• jet length determines 110110 specified in m;
• abrasive granularity determines 0011000 specified in mm;
• abrasive consumption determines 1110111111 specified in kg/m^2;
• the process productivity determines 111111111 specified in m^2/h.

These factors after transformation into a decimal system in accordance with Equation (1) and after scaling into real numbers in accordance with Equation (2) conforms to the following values of parameters:

• water pressure of 29.28 MPa;
• water consumption of 28.70 dm^3/min;
• feed of 286.97 mm/min;
• jet length of 1.14 m;
• abrasive grain granularity of 0.39 mm;
• abrasive consumption of 9.63 kg/m^2;
• process productivity of 15 m^2/h.

The optimal parameters of corrosive-tarnish removal from steel plate surfaces by means of the high-pressure abrasive-water jet are very similar to the conditions determined by relatively expensive experimental methods [6, 7].

7. Summary

The application of the respective numerical techniques enabled us to design a tool used for optimization of corroded steel plate surfacing by a high-pressure abrasive-water jet. The trained artificial neural network by making use of relations between such input parameters as: the water pressure, the water consumption, the feed, the distance between the sprinkler and the processed surface, the abrasive granularity, the abrasive consumption and the set output parameter, i.e. the process productivity, generated an adequate process model. This model consisting of a series of simple linear mathematic equations was subjected to optimization using the genetic algorithm. Finally such parameter values were generated that ensured the maximum process productivity by the use of abrasive-water jet, which was the objective of the assumed numerical procedure.

Therefore the research procedure revealed the operational effectiveness of the artificial neural network and the genetic algorithm in predicting and optimizing tasks even for such complex technologies as surface machining by the high-pressure abrasive-water jet.

References

[1] Babets K., Geskin E.S.: *Development of a generic procedure for modeling of the waterjet cleaning*, 2001, WJTA American Waterjet Conference, Minneapolis, Minesota, 2001, Paper No. 58.

[2] Babets K., Geskin E.S.: *Application of soft computing techniques for modeling and optimization of water-jet-based surface processing*, 15th International Conference on Jetting Technology, Ronneby, Sweden, 2000, pp. 297–307.

[3] Babets K., Geskin E.S.: *Optimization of jet based material cleaning*, Int. Symposium: New Applications of Water Jet Technology, Isinomaki, Japan, 1999, pp. 197–206.

[4] Borkowski J., Borkowski P.: *Rozkruszanie ziarn ściernych podczas wysokociśnieniowego czyszczenia hydrościernego*. XXIII Naukowa Szkoła Obróbki Ściernej, Rzeszów–Myczkowce, 2000, s. 518–525.

[5] Borkowski P.: *Badania przydatności ścierniwa w wysokociśnieniowym strumieniu hydrościernym*, XXII Naukowa Szkoła Obróbki Ściernej, Gdańsk–Jurata, 1999, s. 87–92.

[6] Borkowski P.: *Selction of peripherial equipment for small vessels corroded surfaces cleaning by highpressure hydroabrasive jet*, Int. Conf. on Water Jet Machining WJM, 2001, Cracow, 2001, pp. 149–158.

[7] Borkowski P.: *The sprinkler optimisation used for high-pressure hydroabrasive cleaning*, Scientific Book of the Department of Mechanical Engineering No. 29: Modern Techniques and Technologies, Technical University of Koszalin, Koszalin, 2001, pp. 27–38.

[8] Kacalak W.: *Wybrane problemy zastosowań sieci neuronowych w technologii maszyn*, Prace Katedr Wydziału Mechanicznego Wyższej Szkoły Inżynierskiej w Koszalinie w zakresie technologii maszyn, posiedzenie Sekcji Podstaw Technologii

Maszyn Komitetu Budowy Maszyn PAN, Koszalin, 1993, s. 28–41.

[9]   Masters T.: *Sieci neuronowe w praktyce*, WNT, Warszawa, 1999.

[10] Meng P., Decaro L.S.M., Geskin E.S., Leu M., Huang Z.: *Mathematical modeling of waterjet cleaning*, 9th American Waterjet Conference, Dearborn, Michigan, 1997, Paper No. 37, pp. 509–523.

[11] Michalewicz Z.: *Algorytmy genetyczne + struktury danych = programy ewolucyjne*, WNT, Warszawa, 1999.

Podstawy modelowania obróbki powierzchniowej wysokociśnieniowym strumieniem wodno-ściernym z zastosowaniem algorytmu genetycznego

Zaprezentowano algorytm genetyczny stworzony do poszukiwania korzystnych warunków czyszczenia wysokociśnieniową strugą wodno-ścierną.

Zadanie to zrealizowano, wykorzystując wyniki eksperymentów obróbki usuwania nalotu korozyjnego za pomocą wysokociśnieniowej strugi wodno-ściernej. Doświadczenia wykonano, używając wysokociśnieniowego pistoletu typu HP 750-2 firmy WOMA, uzbrojonego w tryskacz z wielootworową dyszą koncentryczną. Stosowano przy tym hydromonitor zasilany silnikiem elektrycznym (94 kW), który wytwarza strumień wody o ciśnieniu do 75 MPa. Badania empiryczne opierały się na wykorzystaniu takich parametrów obróbki jak: ciśnienie wody w przedziale 20–30 MPa, wydatek wody 25–40 dm^3/min, posuw 250–400 mm/min, odległość tryskacza od powierzchni obrabianej 0,8–1,2 m, ziarnistość ścierniwa 0,2–1,2 mm, wydatek ścierniwa 4–10 kg/m^2 oraz wydajność obróbki 10–15 m^2/h.

Na ich podstawie powstała baza danych, spośród których wyodrębniono 352 przypadki przydatne do odpowiedniego doboru i uczenia sieci neuronowej. Aby znaleźć najlepszą sztuczną sieć neuronową, przebadano ich kilka tysięcy i okazało się, że najbardziej zadowalające rezultaty dała sieć o strukturze liniowej. W jednej z nielicznych do nauczenia można było zastosować wszystkie parametry jako neurony wejściowe. Do nauczenia sieci użyto metody pseudoinwersji. Otrzymany model składający się z szeregu prostych zlinearyzowanych równań matematycznych został zoptymalizowany za pomocą algorytmu genetycznego, który umożliw-wił określenie wartości optymalnych.

Algorytm genetyczny pracował na chromosomie składającym się z 67 bitów. Dzięki niemu wygenerowano wartości parametrów, zapewniających maksymalizację wydajności obróbki powierzchniowej skorodowanych blach stalowych realizowanej przy użyciu wysokociśnieniowej strugi wodno-ściernej, co było celem nadrzędnym przyjętej procedury numerycznej. I tak: ciśnienie wody wyniosło 29,28 MPa, wydatek wody 28,70 dm^3/min, posuw 286,97 mm/min, odległość 1,14 m, ziarnistość ścierniwa 0,39 mm, wydatek ścierniwa 9,63 kg/m^2. Procedura badawcza wykazała skuteczność działania sztucznej sieci neuronowej oraz algorytmu genetycznego w zadaniach prognostycznych i optymalizacyjnych nawet tak złożonych technologii jak powierzchniowa obróbka wysokociśnieniową strugą wodno-ścierną.

Physical basis of surface treatment with high-pressure cryogenic multiphase liquid jet

P. BORKOWSKI

Technical University of Koszalin, Racławicka 15-17, 75-620 Koszalin

The paper presents theoretical analysis of dry-ice grains (CO_2) behaviour in a high-pressure multiphase liquid jet. The velocities of ice grains at the cryo-sprinkler outlet and in the collision zone were calculated. Their kinetic energy and thermodynamic properties of water-ice jet were also calculated. Experiment methodology concerning two test stands, cryo-sprinkler and dry-ice (CO_2) pellets characteristics were discussed. The results obtained allow us to establish specific surface treatment mechanism using such water-ice jet. Very explosive dry-ice sublimation in the collision zone and cleaning process wavy character were also stated.

Keywords: *cryogenic jet, high-pressure water-ice jet, multiphase jet, surface cleaning*

1. Introduction

Surface treatment using the high-pressure cryogenic multiphase liquid jet consists in bulk micro-treatment of the surface with ice-grains transported with a water jet. Due to high rate of this jet, often aerated to considerable degree, the ice-grains gain the energy necessary to perform a treatment operation.

A number of the surface-processing technologies based on the use of the air-ice stream [25, 26] have been previously suggested. The adoption of the ice-jet technology is determined by the effectiveness of the generation and handling of ice abrasives [12, 14, 24].

A noticeable interest in high-pressure cryogenic jets [9, 16, 17], abrasive-cryogenic jets [10, 16, 22] and ice jets [15, 19, 27] has been aroused in recent years. A high-energy ice jet is created by ice particles driven by a stream of air [13, 21], other gas [2, 3, 6] or water [1, 19, 20] displaced with a great velocity. Ice particles, indispensable components of jets, are produced by crushing the larger ice particles [12, 20] or are obtained from dry-ice pellets [26, 29].

Nowadays this technology of ice generation is in widespread use [25, 28]. Usually dry-ice pellets are accelerated by compressed air [11, 30], hence the components of this ice jet escape into the atmosphere leaving merely particles of disposable impurities.

It is possible to increase the efficiency of cleaning with a jet including dry-ice pellets, especially when fairly hard impurities are to be disposed of, making use of a

high-pressure cryogenic water jet. Thus this paper is devoted to investigations of the physical basis and suitability of a high-energy water-air-ice jet.

2. Theoretical analysis

It is possible to assess the phenomena occurring in the process of surface treatment with the high-pressure cryogenic multiphase liquid jet and to determine its physical principles by analyzing the quantities describing dynamics of individual ice grains. However, this analysis is impeded by rapid interactions of ice grains, irregularity of their shapes, solid geometry and other quantities that vary quickly. Taking the above into consideration, the behaviour assessment of ice grains in the high-pressure multiphase water-air jet could be carried out using the model calculations.

A spherical shape of the ice grain was assumed within the theoretical framework. Assuming that about 100% shapes of dry-ice (CO_2) grains could be circumscribed with a cylinder [1, 25, 26] an effective radius of a model spherical grain must be calculated comparing the volume of a cylinder with a sphere. That radius is then given by the expression:

$$r = 0.5 \cdot \sqrt[3]{1.5 \cdot h \cdot d^2} \,, \tag{1}$$

where h, d are the cylinder height and diameter, respectively (ice grain size).

The sprinkler with a multioutlet concentric nozzle, whose optimized construction is discussed in [8], is necessary for an effective cryogenic multiphase liquid jet cleaning. Therefore, the present theoretical analysis of the behaviour of dry-ice (CO_2) grains during their acceleration and interaction with the material was designed for such a sprinkler with a concentric nozzle [5].

2.1. Velocity of dry-ice grains

The theory based on fluid mechanics laws was used to determine the value of ice grain acceleration. According to this theory, the aerodynamic resistance of model dry-ice grains with the radius r moving in viscous liquid, e.g. the water jet of different aeration, could be obtained by solving the following equation:

$$F_D = C_D \frac{\rho_w (u-v)^2}{2} \pi r^2 \,, \tag{2}$$

where:
  C_D – drag coefficient of grains moving in a multiphase liquid stream,
  ρ_w – medium (jet) density,

    u – high-pressure multiphase liquid stream velocity,
    v – ice grain velocity in a stream,
    r – radius of a model spherical ice-grain.
    The thrust force F_N of a jet exerted on ice grain causes its acceleration. The value of this force is given by the following relation:

$$F_N = \frac{4}{3}\pi r^3 \rho_i \frac{dv}{dt},$$ (3)

where ρ_i is the dry-ice CO_2 density.

    Under steady-state conditions of fluid flow, the thrust force of a jet counterbalances the aerodynamic resistance of ice grains causing its acceleration. Thus the right-hand sides of equations (2) and (3) could be considered to be equal. Then, introduction of a constant:

$$K = \frac{8}{3}\frac{r}{C_D}\frac{\rho_i}{\rho_w}$$ (4)

gives the following expression describing the ice grain acceleration in a jet:

$$\frac{dv}{dt} = \frac{(u-v)^2}{K}.$$ (5)

    The same relationship describes the abrasive grain acceleration in the high-pressure hydroabrasive jet used for cutting [23]. Assuming the boundary conditions $t = 0$ and $v = 0$ after integrating equation (5), we arrive at the following approximate formula describing the velocity of ice grains moving in a steady-state jet:

$$v = \frac{u^2 t}{ut + K}.$$ (6)

In this relationship, the high-pressure water-jet velocity is [5]:

$$u \cong 14\sqrt{10 p_n},$$ (7)

where p_n [MPa] is a water pressure. The time of ice-grain flow out of the sprinkler tube present in Equation (6) can be defined by the quotient of tube length and water jet flow velocity.

    Based on the above assumptions, the dry-ice grain velocity at the sprinkler tube outlet was calculated. A few examples of these calculations (Figure 1) show that the

ice-grain velocity is considerably reduced as the water pressure and its content in a jet being aerated decrease. A comparison of these results and flow rates of air-jet driven ice grains presented in the last position of the diagram testifies to the advantages of a water medium in a high-pressure jet. The influence of the water pressure on the ice-grain velocity at the sprinkler tube outlet (of different length) is shown in Figure 2.
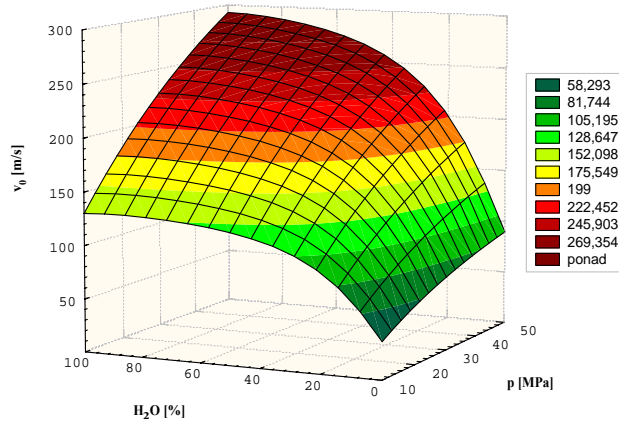
Fig. 1. Influence of water content in a jet and water pressure on the velocity at the sprinkler tube outlet (L_T = 200 mm) for dry-ice (CO_2) grains

Taking into account the effect of the high-pressure cryogenic multiphase liquid jet on the workpiece, its flow velocity is of a great importance. Furthermore, the jet at the outlet encounters the air resistance hampering its flow and intensifying its scattering. Thus, deceleration in the jet flow rate is expressed by the formula:

$$a = \frac{v_0^2}{2L_m},$$
(8)

where:
   v_0 – jet flow velocity at a sprinkler outlet,
   L_m – jet reference length.
   The flow velocity at a random cross-section of the water-ice jet is described by the following relation [7]:

$$v = v_0 \left(\frac{D_0}{D} \right)^2 \sqrt{1 - \frac{L}{L_m}},$$
(9)

where:

v_0 – jet flow velocity at a sprinkler outlet,
D – jet diameter at a cross-section under consideration,
D_0 – jet diameter at a sprinkler outlet,
L – distance from a sprinkler tube outlet to a considered cross-section,
L_m – jet reference length.
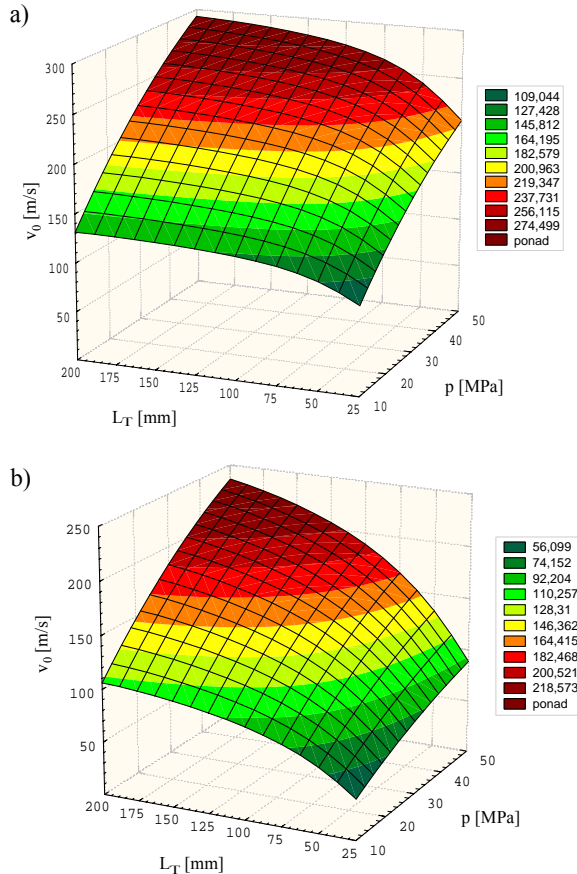
Fig. 2. Influence of different sprinkler tube lengths (L_T) and water pressure (p) on water-ice jet velocity. Water content in a jet: a) 100%; b) 30%

It is possible to determine the quantities D, D_0, L_m included in this formula only by the experimental method [5].

Based on relationship (9) the appropriate calculations of the high-pressure cryogenic multiphase liquid jet flow velocity in a zone of collision with the workpiece were carried out. Examplary results of the flow-velocity calculations for dry-ice CO_2 grains in the working zone, whose distance from the sprinkler tube outlet ($v_{0.5}$) is

0.5 m are presented in Figure 3 and Figure 4. It is evident that an increase in the sprinkler tube length and the rated water pressure causes an increase in the ice-grain velocity.
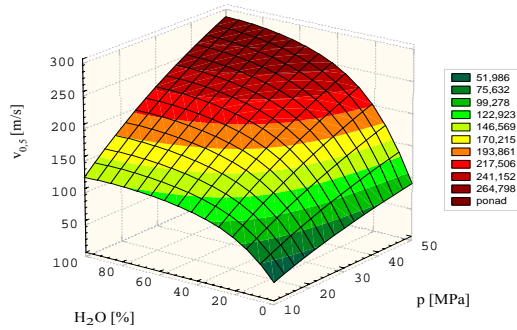
Fig. 3. Influence of water content in a jet and water pressure on the dry-ice (CO_2) grains velocity in the erosion area for sprinkler tube length $L_T = 200$ mm
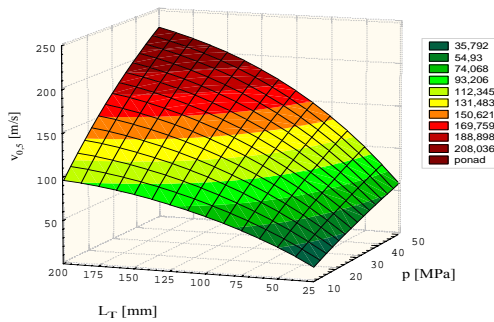
Fig. 4. Influence of the sprinkler tube length and water pressure on the velocity in the erosion area for dry-ice (CO_2) grains moving in jet of 30% water content

These investigations allowed a crucial practical conclusion that the ice-grain velocity both at the sprinkler tube outlet and in the treatment zone only slightly depended on the intensity of water-jet aeration.

2.2. Kinetic energy of dry-ice grains

Making use of the above dry-ice grains flow velocity it is possible to calculate their kinetic energy E_K in the cutting zone as well, according to the following expression:

$$E_K = \frac{2}{3}\pi r^3 \rho_i v_{0.5}^2 .$$
(10)
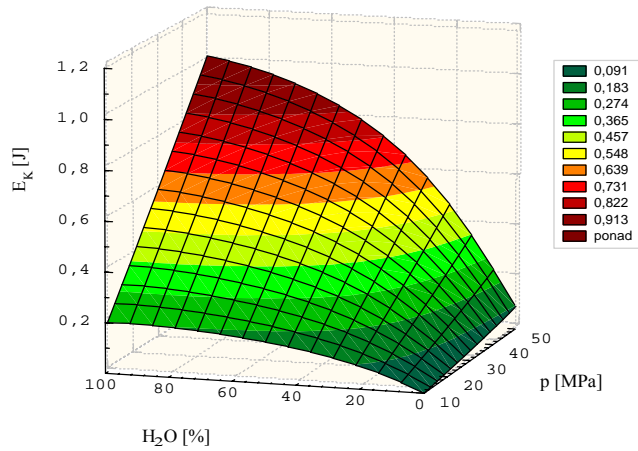
Fig. 5. Influence of water content in a jet and water pressure on the kinetic energy for dry-ice (CO_2) grains ($L_T = 200$ mm)
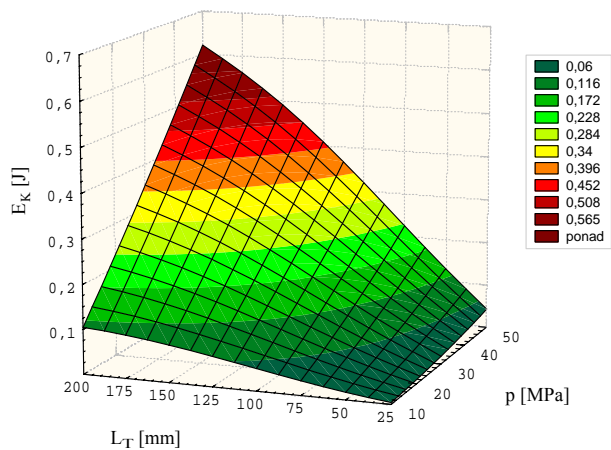
Fig. 6. Effects of the water pressure and the sprinkler tube length on the kinetic energy for dry-ice (CO_2) grains carried by jet of 30% water content

Diagrams of kinetic energy of dry-ice grains in the cutting zone, whose distance from the sprinkler tube outlet is 0.5 m, are plotted on the basis of the above formula in Figure 5 and Figure 6. They show that an increase in the sprinkler tube length, water content in a jet being aerated and the water pressure cause a considerable increase in the kinetic energy of dry-ice grains. The above results revealed that the kinetic energy of abrasive grains accelerated by means of water is over 15 times higher compared with the energy of grains accelerated by the compressed air jet.

2.3. Thermodynamic properties of high-pressure liquid jet

The high quality of dry-ice pellets [25, 26] and the lowest temperature of a high-pressure water jet acquire importance due to an increase in the efficiency of cleaning. Taking this into consideration the thermodynamic conditions of dry-ice pellets associated with the formation of a high-pressure water-air-ice jet should be analysed. Therefore theoretical analysis of pneumatic conveying of ice particles from an ice hopper to a sprinkler and their mixing and acceleration in a high-pressure water-air jet should be undertaken. A series of simplifying assumptions should be made in order to determine the temperatures of individual dry-ice pellets in contact with the treated surfaces. Constant temperature of water-jet, while conveying the ice particles from an ice hopper to a sprinkler, and thermal stability in a high-pressure water jet, while mixing with ice particles in a cryo-sprinkler and their convection to a collision zone in the treated material were assumed as a main technical simplification. It was also assumed that the mass, volume, cylindrical shape and morphology of the surface of ice particles examined in these circumstances did not change.

Accepting the above assumption, a quantity of heat taken up by each ice particle can be expressed – according to Newton's principle – by the equation:

$$Q = \int_0^{t_k} \alpha_1 (T_i - T_a) dA dt + \int_{t_w}^{t_k} \alpha_2 (T_i - T_w) dA dt, \tag{11}$$

where:

α_1, α_2 – coefficients of warm uptake during pneumatic transportation (α_1) and accelerating in water stream (α_2),

A – surface of ice grain,

T_i – temperature of ice grain,

T_a, T_w – temperature of aerial and water environments, respectively,

t – time,

t_k – entire time of ice flow from hopper to workpiece,

t_w – time of ice grains contact with high-pressure water jet.

As is well known, thermal energy brings about a rise in the temperature of ice pellets. The following relation can determine this temperature of ice pellets:

$$Q = -c_p \rho_i \left(\int_0^{t_k} \frac{\partial T}{\partial t} dV dt + \int_{t_w}^{t_k} \frac{\partial T}{\partial t} dV dt \right), \tag{12}$$

where:

c_p – specific heat of ice,

ρ_i – ice density,

V – volume of ice grain,

$\dfrac{\partial T}{\partial t}$ – speed of rise in the ice grains temperature.

The coefficients α_1 and α_2 in Equation (11) can be defined according to the following empirical dependencies [18]:

• during pneumatic transportation of ice grains through the smooth-surface hose

$$\alpha_1 = 4.8 + 3.4v, \tag{13}$$

• during transportation of ice grains in the high-pressure water jet

$$\alpha_2 = 300(1 + 6\sqrt{v}). \tag{14}$$

Moreover, earlier empirical calculations presented in the paper [1] revealed that due to thermodynamic conditions during high-pressure water jetting the second part of equation (11) is 4.921 times greater than the first one.

Taking into consideration the above dependencies (13) and (14) in Equation (11) and comparing them with Equation (12), it is possible to calculate the end temperature of the ice-grain surface in the collision zone. As a result of thorough empirical analysis [1] of the thermodynamic properties of all media involved in the process of creation of a high-pressure water-air-ice jet, the impact of surface temperature of ice pellets onto the surface of the material could be determined by the following equation:

$$T_i = T_0 - \frac{A\Delta T_i t_k \left(4.8 + 0.85\dfrac{v_a^2}{L}t_k\right) + 300A\Delta T_w\left(t_k - t_w\right)\left(1 + 6\sqrt{v_k}\right)}{5.921c_p\rho_i V t_k}, \tag{15}$$

where:
T_0 – temperature of environment of ice grain,
ΔT_i – increase of ice grains temperature heated during pneumatic transportation,
ΔT_w – increase of ice grains temperature heated with high-pressure water jet,
t_k – entire time of ice flow from hopper to workpiece,
t_w – time of ice grains contact with high-pressure water jet,
v_a – speed of air inflow to the sprinkler,
v_k – jet speed in the collision zone of treated material,
L – hose length connecting hopper with cryo-sprinkler.

This equation allowed us to determine the results presented in Figure 7. Analysis of these results showed that an increase in the pressure of water jet caused a drop in the temperature of ice pellets in the zone of collision with the treated material. It applies to all technological conditions of creation of a high-energy water-ice jet. Under standard

conditions of this jet creation the temperature of ice pellets was slightly higher compared to the temperature of precooled water and air which could be alternately used.
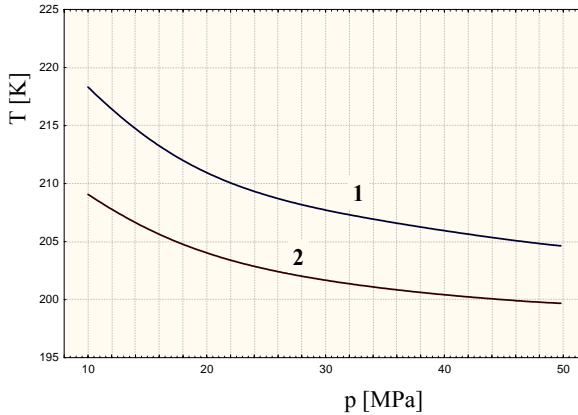
Fig. 7. Water pressure influence on the temperature of dry-ice pellets in the collision zone.
Water jet: 1– normal, 2 – precooled

Therefore the ice pellets obtained in the precooled high-pressure system were of higher quality. So it is worth making efforts to insulate the main subassemblies of technological equipment and precool the process water and even air used for mass transport of ice pellets from the hopper to the cryo-sprinkler.

3. Research methodology

Experiments were carried out on two special test stands equipped with instrumenttation, whose principal view is presented in Figure 8. The first stand (Figure 8a), i.e. own-made hydromonitor being built on the basis of the Hammellmann high-pressure pump of HDP 164 type, allows us to obtain nominally the water jet pressure reaching 330 MPa and the water flow rate of 28 dm³/min. The other one (Figure 8b) presents electric hydromonitor characterized by the maximum water pressure p equal to 75 MPa and water flow rate of 75 dm³/min. A high-pressure gun equipped with a cryo-sprinkler (Figure 9) with a four-outlet concentric nozzle with water jets $d_w = 1.2$ mm in diameter, a tube $D_k = 22$ mm in diameter and $L_k = 200$ mm in length was used in these experiments. This sprinkler is different in design from the previous one [8] mainly due to characteristics of the concentric nozzle and external and internal insulating inserts.

Dry-ice pellet grains stored in special cases (Figure 10) with heat exchanger installations inside are prepared for technological water and air cooling, which warrants ice-grains transportation. New design features applied to a high-pressure water supply system for a test stand and a sprinkler made the temperature of process water lower. Owing to that the temperature in the zone of mixing with dry-ice pellets

was as low as 15 ^{o}C, whereas in the case of common equipment it was much higher, i.e. ca. 43 ^{o}C. During the tests the water-jet pressure p was changed in the range from 20 to 330 MPa.

a)

b)
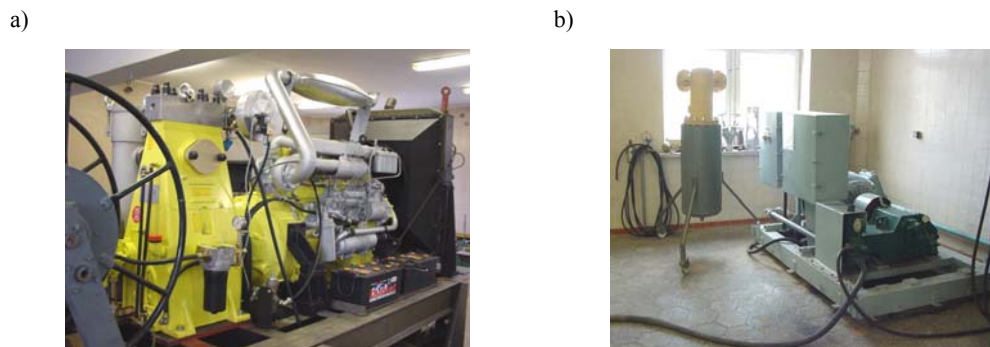
Fig. 8. General view of two test stands based on a hydromonitor with a high-pressure pump:
a – HAMMELMANN, b – WOMA and a control system with a dry-ice pellet hopper

a)

b)

c)
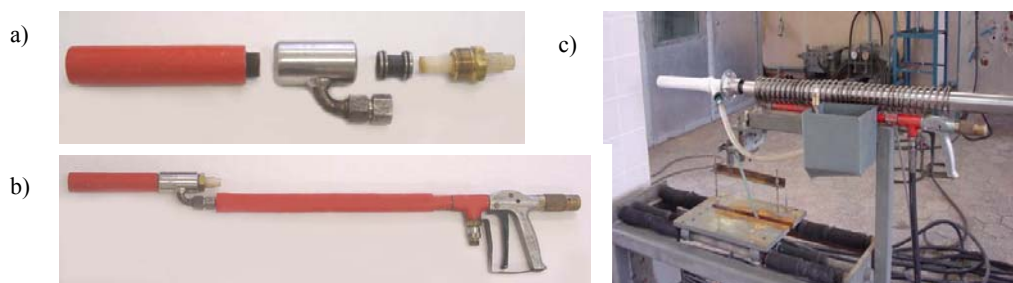
Fig. 9. The cryo-sprinkler view (a), high-pressure gun (b) and test stand (c)
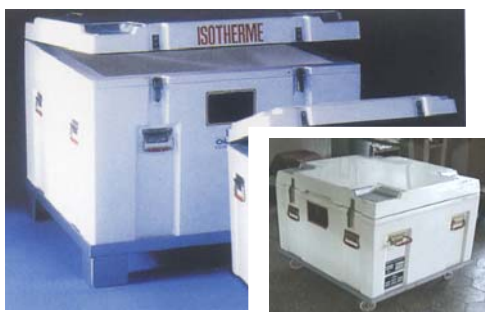
Fig. 10. Isothermal cases used for high-pressure hydro-jet installation cooling and dry-ice CO_2 pellet transportation

A high-pressure water jet was mixed in a sprinkler with dry-ice pellets (Figure 11) made according to German technology [26, 28, 30]. The particle-size distribution is the result of different jet pressures: 41% of the particles in the range of 1 mm, 31% in the range of 2 mm and 28% in the range of 3 mm. This means an average particle diameter of 1.87 mm for those particles in the dry-ice free jet which are relevant to the removal process [25, 29]. The dry-ice pellets were also accelerated with air jets at the pressure of 0.3, 0.5, and 0.7 MPa in order to compare the effects of processing.
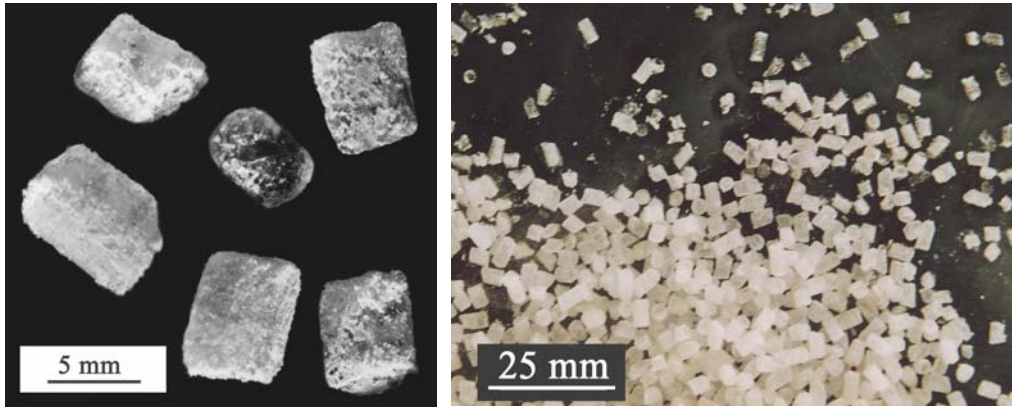
Fig. 11. Dry-ice CO_2 pellets made according to German technology

The high-pressure water-ice jet configured in this way was used for processing about a dozen different types of materials such as metal plates (steel, aluminum, copper and lead), plastics, PVC materials, plexiglass, glass, ceramics, different rock materials, rubber, etc. The surface of the above materials differed in quality because apart from their natural state they were passivated, corroded and also coated with paint or asphalt (izohan type), either rubberized or glue spread etc. Lead, which is charactreized by high ductility, was most often used for testing the course of erosion mechanism with this sort of water-ice jet.

Quality and a degree of surface erosion of processed materials were assessed by means of different measuring instruments, including:

- scanning electron microscope JEOL 5500LV,
- stereo-optical microscope MBC-10,
- profilogram CARL ZEISS JENNA ME10, equipped with special attachments such as T8S and T10S.

4. Effects of surface cleaning

From among different effects of surface cleaning observed during the studies only mechanisms of cleaning process and also their conditions and efficiency for different materials are discussed here.

4.1. Mechanisms of surface treatment

The studies confirmed that regardless of substrate material the coatings that are characterized by high adhesiveness are more resistant to removal than the coatings weakly bonded to the surface. It is evident that if the high-energy water-air-ice jet is used for cleaning, the main mechanism of surface treatment consists in hydrodynamic impact of dry-ice grains and water on the material as it was being removed. However, the mechanism of material removing from surfaces by the high-pressure water-ice jet is very complicated. The most characteristic feature of the high-pressure cryogenic liquid jet affecting the work surface relies on multiple impingements of jet droplets, together with dry-ice grains transported, on this surface, which results in formation of stresses that vary quickly. A fatigue character of these stresses contributes to the surface cracking, usually dispersing in different directions. The most decisive effects on the intensity of this process produce the dry-ice (CO_2) grains forming effective tool-points attacking the work surface with great energy. Dry-ice pellet (CO_2) particles, crumbled away during surface treatment, penetrate into the dirt layer and then sublimate enlarging their volume by ca. 500 times. Sudden character of that process is nearly explosive, while the treatment zone is smoky by condensating CO_2.

a) b) c)
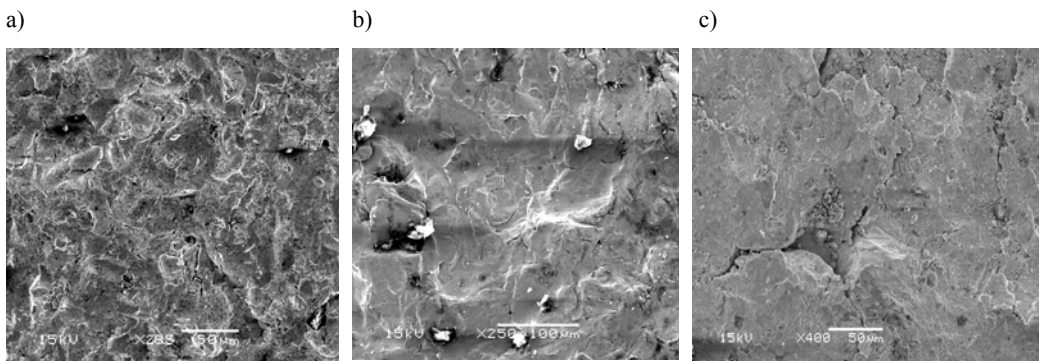
Fig. 12. Surface (lead) treated which high-pressure abrasive-water jet (a) and high-energy dry-ice pellet jet accelerated by: b – water at the pressure of 20 MPa, c – compressed air (p = 0.7 MPa)
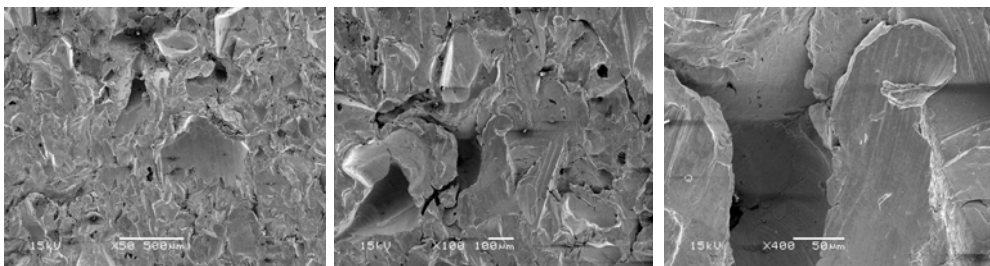
Fig. 13. Surface treated which high-energy hybrid jet with exposed loosened chips of eroded lead material

Water is also important in this process, as it not only induces cavitational erosion, but also is a medium that penetrates the cracks obtained, causing disaggregation of the material. This mechanism generally results in a uniform spalling of particles splitted off the workpiece surface.
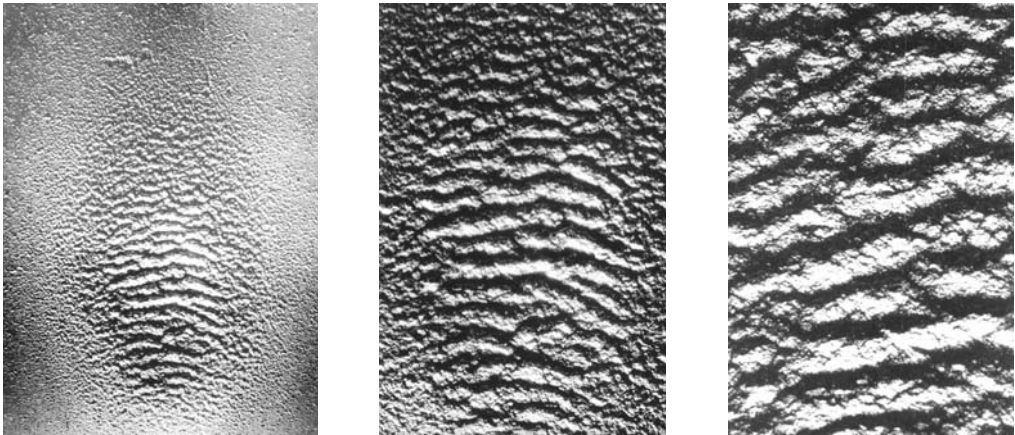
Fig. 14. Example of the surface (lead) after treatment which high-energy water-ice jet, showing a wavy character of erosion

Dry-ice pellets behave in the way similar to abrasive grains, which is shown in SEM micrographs of treated surface (Figure 12). However, this causes that the impact of ice particles is significantly weaker compared to that of abrasive grains. This can be exemplified by SEM micrographs of the surface treated with a high-pressure hybrid jet (Figure 13) comprising abrasive and ice grains admixed in different phases of forming this erosive tool [4].

Analyses of the mechanisms of surface treatment with a high-energy water-air-ice jet also confirmed a distinctly wavy character of erosion. It is illustrated in Figure 14. However, these investigations did not confirm the essential effect of cryogenic shrinkage of coatings, which could intensify the decoating process.

4.2. Condition and efficiency of cleaning process

A high-energy water-air-ice jet is formed of a few water jets discharged from outlets of a multioutlet concentric nozzle. A concurrent flow of these water jets through a sprinkler tube causes the central outlet of the concentric nozzle to suck in air along with ice particles. The water-air-ice jet obtained in such a way has fairly homogeneous structure and while discharging from the sprinkler tube affects the treated surface with high energy (Figure 15). It results in impurities removal or stripping coatings from material surfaces and intensive sublimation of dry ice. Therefore it makes the processing zone and adjacent area mostly "smoky" which is shown in Figure 16.

Fig. 15. Influence of a high-energy water-ice jet on a workpiece in an erosive area

Fig. 16. Intensity of "smokiness" formed by sublimating dry-ice CO_2 pellets
in a cleaning area while testing

Consumption of water and dry-ice pellets during the trade off studies concerned with cleaning the corroded surfaces of steel plates using the water-air-ice jet ranged from 40

to 55 dm^3/min and from 2.3 to 2.8 kg/min, respectively, which is equivalent to the flow intensity of about 1500–2000 dry-ice grains per second. It ensured satisfacto-ry surface processing for these plates with maximum efficiency from 0.35 to 0.45 m^2/h. For the sake of comparison, the ice consumption, while accelerating the ice grains with compressed air in various experimental conditions, ranged from 0.5 to 1.1 kg/min; however, the efficiency of processing was less than ten times lower.

A high-energy water-air-ice jet because of its more favourable process conditions was used for cleaning the surfaces of various materials. Results of these experiments [1] prove that the most efficient is varnish coating cleaning of the glass and steel sheet, especially lead surfaces. Also good effects are obtained for cleaning such surfaces of different plastic and rubber glue layers (coatings).

5. Conclusions

Theoretical analysis of dynamic and thermodynamic issues dealing with the behaviour of dry-ice grains (CO_2) in a high-pressure cryogenic multiphase liquid jet and the previous preliminary experiments on decoating and cleaning the surfaces of different materials allowed the following more general conclusions:

• Effectiveness of surface treatment with a high-energy water-air-ice jet depends on the quality of ice grains. For this reason it is recommended to use the ice of the highest quality with possibly uniform and smooth surfaces and sharp edges and possibly the lowest temperature of a high-pressure water jet, so that the quality of ice particles accelerated with it declines as slowly as possible.

• The dominant mechanism of output, while cleaning with a high-pressure water-air-ice jet, is a hydrodynamic impact of dry-ice CO_2 grains causing explosive dry-ice grains sublimation on the material, hence determining distinctly wavy character of erosion.

• Satisfactory effects of cleaning the surface with high-energy water-ice jet were obtained at the temperature of water not exceeding 288 K, at the pressure p equal to 30 MPa and at the water consumption Q_w ranging from 40 to 55 dm^3/min and ice consumption Q_i in the range of 2.3 to 2.8 kg/min. Under these circumstances the rate of cleaning the corroded steel plates can reach 0.35–0.45 m^2/h, which is almost ten times more efficient than cleaning with a ice jet brought up to speed by compressed air.

• In order to increase the efficiency of surface treatment with a high-energy water-air-ice jet, one should increase the overcooling of ice, which thus is characterised by more favourable morphology, and use the high-pressure water-hybrid jet comprising not only the ice particles, but also grains of proper abrasive material.

References

[1] Borkowski J., Borkowski P.: *Chosen issues of creation and application of high-pressure water-ice jet,* Int. Conf. on Water Jet Machining, Cracow, 2001, pp. 127–140.

[2] Borkowski J., Borkowski P., Czyżniewski A., Lenz Z.: *Badania kriogenicznego wysokoci-śnieniowego strumienia płynu jako potencjalnego narzędzia erozyjnego,* Konferencja: Podstawy i Technika Obróbki Ubytkowej, Koszalin-Unieście, 1994, s. 91–92.

[3] Borkowski J., Borkowski P., Czyżniewski A., Lenz Z.: *Badania możliwości stosowania kriogenicznego wysokociśnieniowego strumienia płynu jako potencjalnego narzędzia erozyjneg*, I Forum Prac Badawczych: Kształtowanie części maszyn przez usuwanie materiału, Koszalin, 1994, s. 288–298.

[4] Borkowski J., Perec A., Borkowski P., Budniak Z., Chomka G.: *Teoretyczne i do-świadczalne podstawy intensyfikowania obróbki wysokoenergetyczną hybrydową strugą hydrościerną*, Grant Komitetu Badań Naukowych, nr 8 T07D 027 20, 2001.

[5] Borkowski P.: *Optymalizacja konstrukcji koncentrycznej dyszy wielootworowej z uwagi na użytkowe właściwości wysokociśnieniowego strumienia hydrościernego*, praca doktorska, Politechnika Koszalińska, Koszalin, 1997.

[6] Borkowski P.: *Teoretyczne podstawy kreowania kriogenicznej strugi erozyjno-ściernej*, XXIV Naukowa Szkoła Obróbki Ściernej, Kraków, 2001, s. 107–114.

[7] Borkowski P.: *Theoretical basis of surface machining with high-pressure hydroabra-sive jet*, Scientific Publication of Mechanical Department: Modern Techniques and Technologies, Technical University of Koszalin, Koszalin, 2001, No. 29, pp. 14–26.

[8] Borkowski P.: *The sprinkler optimisation used for high-pressure hydroabrasive cleaning*, Scientific Publication of Mechanical Department: Modern Techniques and Technologies, Technical University of Koszalin, Koszalin, 2001, No. 29, pp. 27–38.

[9] Chen F.L.: *Introduction of a new precision cryogenic icejet system for processing materials*, Proc. of the 6th Pacyfic Rim Int. Conf. on Water Jet Technology, Sydney, Australia, 2000.

[10] Dunsky C.M., Hashish M.: *Observations on cutting with abrasive-cryogenic jets*, Proc. of the 13th International Conference on Jetting Technology – Applications and Opportunities, Sardinia, 1996, pp. 679–690.

[11] Elbing F., Axmann B.: *Strahlverfahren,* ZWF, Vol. 92, 1997, nr 3, s. 76–77.

[12] Gałecki G., Vickers G.W.: *The development of ice-blasting for surface cleaning*, Proc. of the 6th International Symposium on Jet Cutting Technology, Surrey, U.K., 1982, paper B-3, pp. 59–78.

[13] Geskin E.S., Goldenberg B., Shishkin D., Babets K., Petrenko K.: *Ice based deconta-mination of sensitive surfaces,* Proc. of the 15th International Conference on Jetting Technology, Ronneby, Sweden, 2000, pp. 219–228.

[14] Geskin E.S., Shishkin D., Babets K.: *Application of ice particles for precision cleaning of sensitive surfaces,* Proc. of the 10th American Waterjet Conference, Vol. I, Huston, Texas, 1999, pp. 315–333.

[15] Geskin E.S., Tishmenetskiy L., Li F., Meng P., Shishkin D.: *Investigation of icejet machining*, Proc. of the 9th American Water Jet Conference, Vol. I, Dearborn, Michigan, 1997, pp. 281–290.

[16] Hashish M., Dunsky C.M.: *The Formation of Cryogenic and Abrasive-Cryogenic Jets,* Proc. of the 14th International Conference on Jetting Technology, Brugge, Belgium, 1998, pp. 329–343.

[17] Kiyohashi H., Hanada K.: *A study of production of ice particles by the heat of vapori-zation of cryogenic liquefied fuels and their application in ice jets, and so on*, Proc. of the International Symposium on New Applications of Water Jet Technology, Ishinomaki, Japan, 1999, pp. 51–60.

[18] Kuchling H.: *Physik*, VEB Fachbuchverlag, Leipzig, 1968.

[19] Li F., Geskin E.S., Tismenetskiy L.: *Development of ice jet machining technology*, Proc. of the 8th American Water Jet Conference, Vol. II, Huston, Texas, 1995, pp. 671–680.

[20] Li F., Geskin E.S., Tismenetskiy L.: *Development of icejet machining technology*, Proc. of the 13th International Conference on Jetting Technology, Sardinia, 1996, pp. 725–734.

[21] Liu B.-L., Liu L.-H., Wu L.: *Research on the preparation of the ice jet and its cleaning parameters*, Proc. of the 14th International Conference on Jetting Technology, Brugge, Belgium, 1998, pp. 203–210.

[22] Liu H.T., Fang S., Hibbard C., Maloney J.: *Enhancement of ultrahigh-pressure technology with LN_2 cryogenic jets*, Proc. of the 10th American Waterjet Conference, Vol. I, Huston, Texas, 1999, pp. 297–313.

[23] Mazurkiewicz M.: *Single abrasive particle and high pressure hydro-abrasive jet performance study*, 1989 SME International Conference and Exposition, Detroit, USA, May 1–4, 1989, paper MR89–442, p. 15.

[24] Shishkin D.V., Geskin E.S., Goldenberg B.: *Development of a technology for fabrication of ice abrasives*, Proc. of the 2001 WJTA American Waterjet Conference, Minneapolis, Minnesota, 2001, Paper No. 27.

[25] Spur G., Uhlmann E., Elbing F.: *Experimental research on cleaning with dry-ice blasting,* International Conference on Water Jet Machining, "WJM `98", Cracow, 1998, pp. 37–45.

[26] Spur G., Uhlmann E., Elbing F.: *Dry-ice blasting for cleaning: process, optimization and application*, Wear, Vol. 233–235, 1999, pp. 402–411.

[27] Truchot P., Mellinger P., Duchamp R., Kim T.J., Ocampo R.: *Development of a cryogenic waterjet technique for biomaterial processing applications*, Proc. of the 6th American Water Jet Conference, Huston, Texas, 1991, pp. 473–480.

[28] Uhlmann E., Axmann B., Elbing F.: *Stoßkraftmessung bejm Strahlen mit CO_2-Pellets*, ZWF, Vol. 93, 1998, Nr 6, s. 240–243

[29] Uhlmann E., Axmann B., Elbing F.: *Trockeneisstrahlen – neue Erkenntnisse durch Hochgeschwindigkeits – Videographie*, JOT, Vol. 38, 1998, Nr 7, s. 46–51.

[30] Uhlmann E., Axmann B., Elbing F.: *Reiningen mit Trockeneisstrahlen in der Austauschmotorenfertigung*, VDI-Z, Vol. 140, 1998, Nr 9, s. 70–72.

Fizykalne podstawy obróbki powierzchni przy użyciu wysokociśnieniowej strugi kriogenicznej płynu wielofazowego

W artykule przedstawiono teoretyczny opis fizykalnych podstaw obróbki powierzchni dokonywanej z zastosowaniem wysokociśnieniowej strugi kriogenicznej płynu wielofazowego. Taka struga składa się głównie z napowietrzonej strugi wodnej, powstającej z wielu strumieni koherentnych, oraz z cząstek suchego lodu CO_2 transportowanych przez strumień zasysanego powietrza. Teoretyczna analiza fizykalnych zjawisk występujących podczas tworzenia strugi kriogenicznej pozwoliła określić rozkłady prędkości ziaren lodowych i ich energii kinetycznej w strefie obróbki, a także termodynamiczne warunki tworzenia takiej wysokociśnieniowej strugi wielofazowej. W wyniku tej analizy stwierdzono, że w strefie obróbki ziarna lodu osiągają prędkości rzędu 150–300 m/s, które nawet przy bardzo dużym napowietrzaniu strugi (do ok. 30% zawartości wody) obniżają się jedynie w nieznacznym stopniu. Dzięki temu energia kinetyczna poszczególnych cząstek lodowych jest bardzo duża, dochodząc – przy ciśnieniu strugi wody rzędu 50 MPa – do poziomu 1 J.

Zaprezentowano także oryginalne oprzyrządowanie i urządzenia technologiczne własnej konstrukcji, w których ciśnienie w strudze dochodzi do 330 MPa i w rezultacie możliwa jest wysokowydajna obróbka hydrostrumieniowa.

Badania czyszczenia powierzchni za pomocą tych urządzeń wykazały, że dominującym mechanizmem urobku jest hydrodynamiczne oddziaływanie ziaren suchego lodu CO_2, które, uderzając o powierzchnię materiału obrabianego, przedostają się pod warstwę zanieczyszczeń, gdzie ulegają sublimacji, powiększając około 500-krotnie swoją objętość. Gwałtowny, nieomal eksplozyjny, charakter tego procesu intensyfikuje skuteczność obróbki, powodując jednocześnie „zadymienie” strefy obróbki skondensowanym gazem CO_2. Równocześnie wysokociśnieniowa struga wody przedostaje się do powstających szczelin, wywołując odspajanie cząstek materiału. Taka erozja ma falisty charakter. Stwierdzono także, że skuteczność obróbki zależy od jakości cząstek lodowych, co narzuca konieczność schładzania wysokociśnieniowej strugi wodnej.

Design of bunch-string tools and its influence on their durability

B. CIAŁKOWSKA

Wrocław University of Technology, Wybrzeże Wyspiańskiego 25, 50-370 Wrocław

The durability and performance of bunch-string tools used for cutting hard ceramics were investigated. The strings were designed in the form of a wire or fibre bunch core in a winding coated with an abrasive layer. The windings were made of various materials wound at a different pitch. Two factors turned out to be critical for the durability of such tools: a constant diameter of the string along its whole length and uniformity of the winding serving as the base for abrasive grit dispersed in a metal binding agent.

Keywords: *bunch string, winding, cutting, technical ceramics*

1. Introduction

The technique of cutting with a solid-metal string suffers from a number of drawbacks. The main problem is that such strings are susceptible to premature rupture (usually occurring at the single joint in the loop), which shortens their life. This adverse effect called for a considerable modification of the design of solid-metal-string cutting tools. After years of experience in the field, we created a new string tool design characterized by high cutting performance and reliability. The main idea behind the new design was that a core made up of several wires or fibres would eliminate the single joint – the place most susceptible to rupture during cutting and bending, whereby the cutting string would be more durable.

Tests showed that the durability of such a cutting string depends mainly on the regularity of its cross-section and the kind of winding which ensures this regularity. This applies to the string's cutting durability (ability) rather than to its tensile and bending strength on the cutting machine's guiding disks.

Bunch strings made of wires (up to 0.3 mm in diameter) or glass, carbonized or aramid fibres, are practically unstretchable. In all these cases, the time to rupture is tens of hours for running at a speed of about 30 m/s on a four-disk cutting machine and it is much longer than the life of the abrasive coating.

At a frequency of about 50 revolutions per second bunch strings survive more than 10^6 bends. This means that their endurance is at least 100 times greater than that of solid-metal strings. But solid-metal strings have a much more uniform cross-section

whereby the contact between the abrasive coating and the cut surface is the same along the whole length of the string. Whereas a bunch string breaks usually in places where its diameter has increased as a result of grazing and tearing of the winding.

Taking all this into account, we manufactured bunch strings with windings made of various materials and investigated the properties of the strings for different winding diameters and pitches.

2. Bunch strings

In all our tests we observed that neither the number of wires or fibres in a bunch nor their diameters (ranging from 0.07 to 0.3 mm) affected the durability of the string. The two factors have a bearing only on the string's final diameter. It is the kind of winding and its pitch which determine the endurance of the bunch string.

The windings were made of different materials and varied in their diameter and pitch. The following materials were used: (i) 0.1 mm $\varnothing$ steel wire (ii) 0.07 mm $\varnothing$ tungsten wire, (iii) kevlar and glass fibres (the bunch's diameter < 0.1 mm) and (iv) 0.16 $\varnothing$ mm polyamide fibre.

The bunch strings (with windings with a pitch of 0.1–0.6 mm) were manufactured on an in-house stand [1]. The strings had the form of:

• 0.1 mm $\varnothing$ steel (OH18N9) wire (7 to 19 wires) bunch cores in windings of different design;

• 0.1 mm $\varnothing$ tungsten wire bunch cores in windings made of similar wire at a pitch of 4–9 mm;

• 0.1mm $\varnothing$ tungsten wire bunch cores of different design, in windings made of 0.07 mm $\varnothing$ tungsten wire at a pitch of 3–6 mm.

The endurance of the cores made of tungsten wires is significantly greater than that of the cores consisting of steel wires. The strings are shown below. The magnification of each of the photographs is 25×.

A bunch string made of 7 steel (S) wires (w), each 0.1 mm in diameter, in a winding (W) made of 0.1 mm $\varnothing$ steel wire at a pitch (p) of 4 mm is shown in Figure 1 a–c. This kind of bunch string is denoted by symbol 7wS0.1WS0.1p4. A similar bunch string, but made of 0.1 mm $\varnothing$ tungsten wires at a winding pitch of 3 mm, is shown in Figure 2.

A pitch of 3–6 mm proved sufficient to ensure regularity of the string's cross-section. However, both the steel and tungsten wire winding would be quickly grazed and would break (Figures 1c and 2c) and consequently, the bunch string would rupture.

To improve the uniformity of the grit-nickel abrasive coating, the manufacturing stand [1] was upgraded so that windings with a smaller pitch could be made. An example of a bare string is shown in Figure 3a. The string after galvanization with abrasive grit and after cutting hard ceramics is shown in Figures 2b and 2c,

respectively. As can be seen in the photograph, the winding with this pitch does not ensure sufficient uniformity of the abrasive coating and the string is liable to rupture.
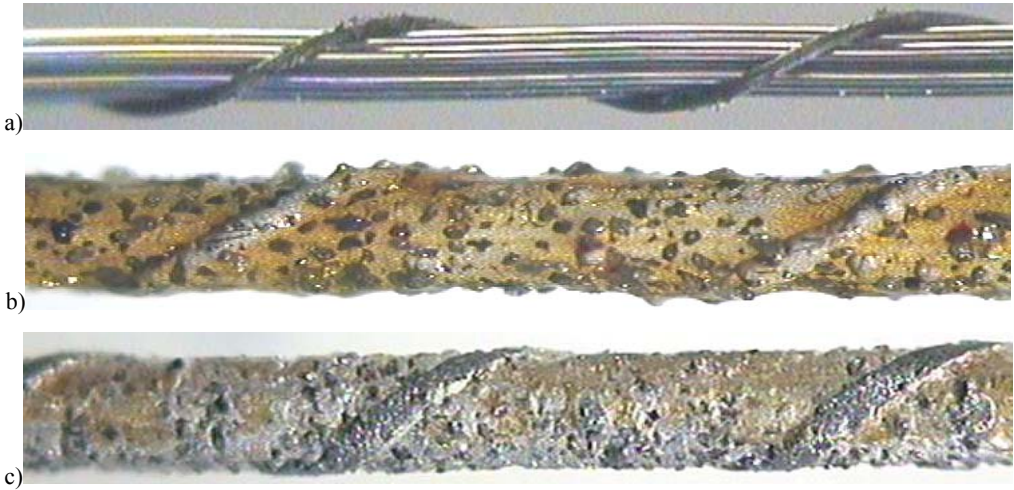
Fig. 1. Steel (S) bunch string, 7 core wires (w), 0.1 mm $\varnothing$ steel (S) wire winding with 4 mm pitch (p) (7wS0.1WS0.1p4): a) before galvanization, b) after galvanization with diamond grit 125/100, c) after cutting silicate ceramics (~1200 mm^2)
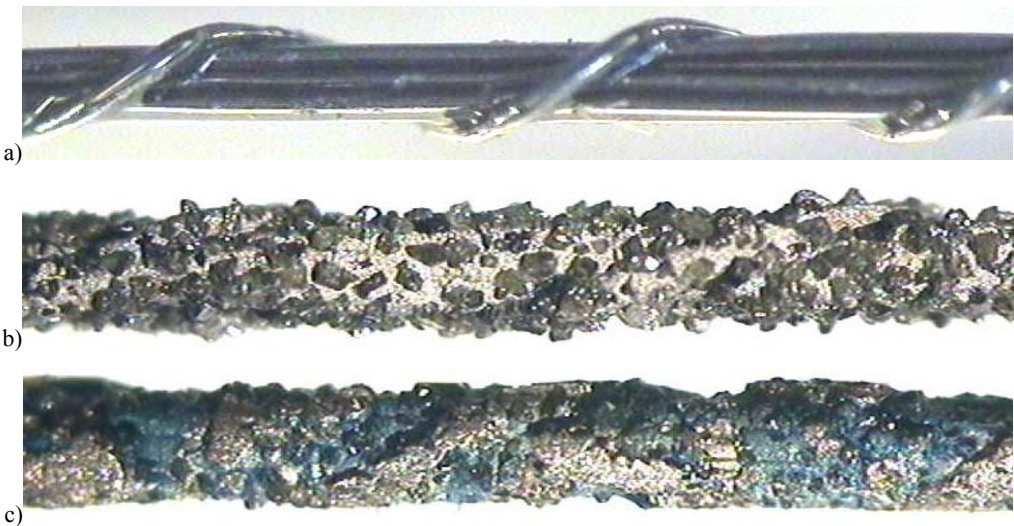
Fig. 2. Tungsten (T) bunch string, 7 core wires (w), 0.1 mm $\varnothing$ tungsten (T) wire winding with 3 mm pitch (p) (7wT0.1WT0.1p3): a) before galvanization, b) galvanization with diamond grit 125/100 dispersed in nickel as binding agent, c) after cutting silicate ceramics (~1200 mm^2)
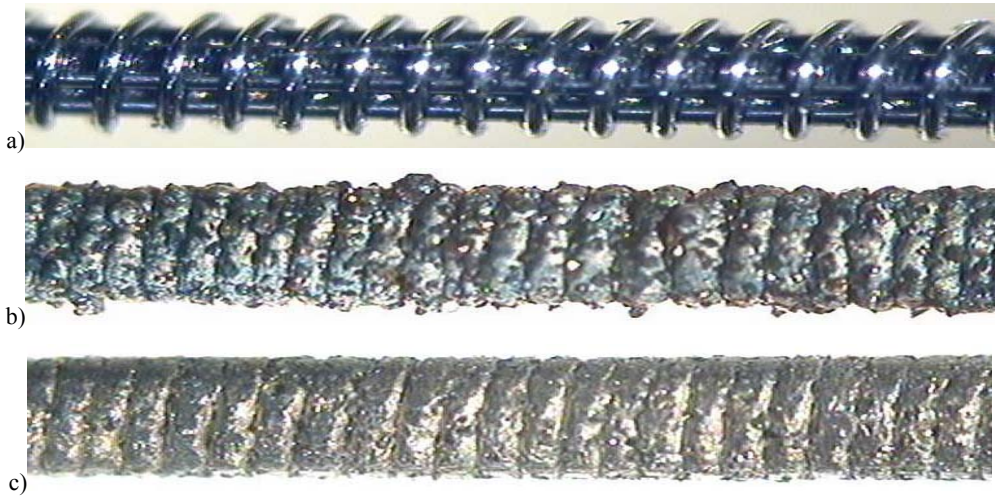
Fig. 3. Tungsten bunch string with steel winding (7wT0.1WT0.1p3): a) before galvanization,
b) after galvanization with diamond grit 125/100 dispersed in nickel as binding agent,
c) after cutting hard silicate ceramics (~1000 mm^2)
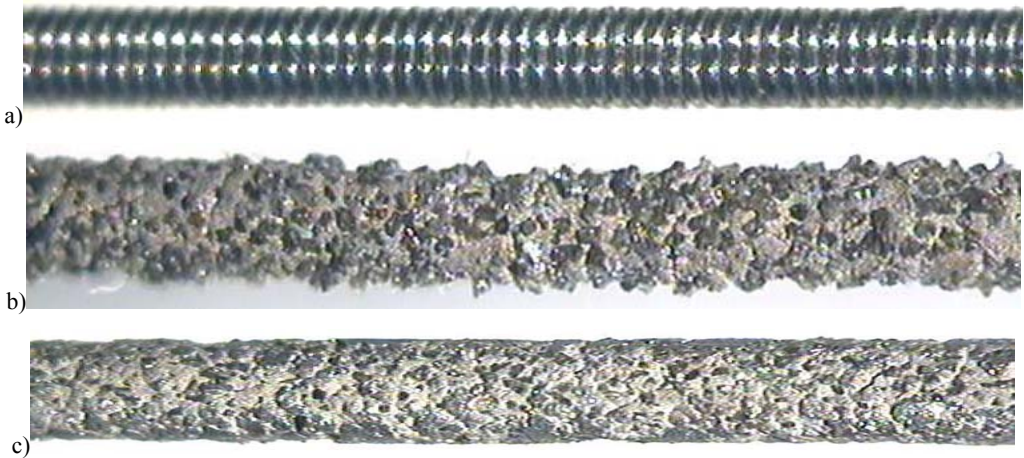
Fig. 4. Bunch string (10wT0.1WS0.1p0.1): a) before galvanization, b) after galvanization with
diamond grit, c) after cutting hard ceramics (~2000 mm^2)

A string with a satisfactorily uniform coating (Figure 4b) and increased endurance
was obtained for a winding pitch of 0.1 mm. The string after heavy use is shown in
Figure 4c. But making such a winding is a laborious process since 25 thousand winds
are needed to cover the 2500 mm long string. Moreover, it is rather difficult to avoid
winding errors which become the string's weak points and eventually cause its rupture.

Fig. 5. Bunch string (7wT0.1WCu0.3p0.6)

None of the windings mentioned above seems to satisfy the condition of string diameter uniformity along the whole length of the string. Consequently, the endurance of the string is limited in each of the cases.

The best results for bunch strings with a tungsten core were obtained when the winding was made of rolled copper strip 0.03–0.1 mm thick and 0.3–1 mm wide. A bunch string with a tungsten core in such a copper strip winding (with a pitch much larger than the strip's width) is shown in Figure 5.

Even when the pitch was only slightly larger than the strip's width (Figure 6a), the abrasive grit-nickel coating was not uniform enough both before galvanization (Figure 6b) and after cutting (Figure 6c). This caused crumbling of the coating – an effect usually followed by a premature rupture.

A bunch string with its winding made of 0.8–1 mm wide copper strip wound at a pitch of 0.6 mm so that the winds overlap (Figure 7a) has the highest endurance. The uniformity of the winding can be further improved by idle running the string in the cutting machine (Figure 7b). A grit-nickel coating was applied by the galvanic method (Figure 7c). The string after several minutes of cutting hard silicate ceramics is shown in Figure 7d.

The brittleness of the metal wires significantly increased after galvanization, which was observed for both steel and tungsten wires, particularly the ones with the smallest diameter (0.07–0.1 mm). This adverse effect can be prevented by using thicker wires (up to 0.3 mm thick) or by covering individual wires with an organic agent before copper strip is wound around the core.

The core in bunch strings can also be made of glass, carbon or aramid fibres. The tensile strength of such a core (0.3–0.8 mm in diameter) is comparable with the strength of a core made from tungsten wires and its fatigue bending strength is even greater.

Polyester, epoxy resin and polyurethane binders were used to make the cores. The polyester and epoxy binders proved impractical since the fibre cores obtained were not elastic enough, despite the fact that highly plastic materials were used. Such cores would often break. The best results were obtained for aramid fibres with a polyurethane binder of low hardness (A40 on the Schore scale). Copper strip was then wound around the polymer (aramid) cores. The copper winding was compacted by idle running the string in the cutting machine.
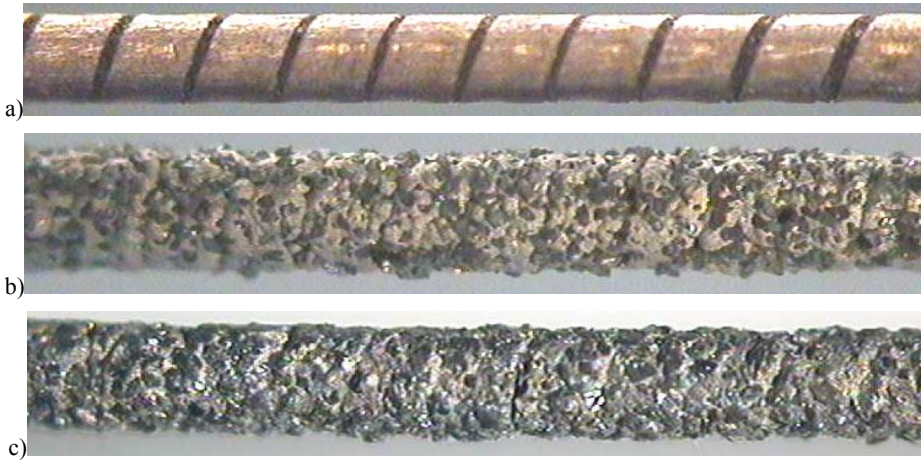
Fig. 6. Bunch string (7wT0.1WCu0.3p0.4): a) before galvanization, b) after galvanization
with diamond grit, c) after cutting hard ceramics (~1500 mm^2)
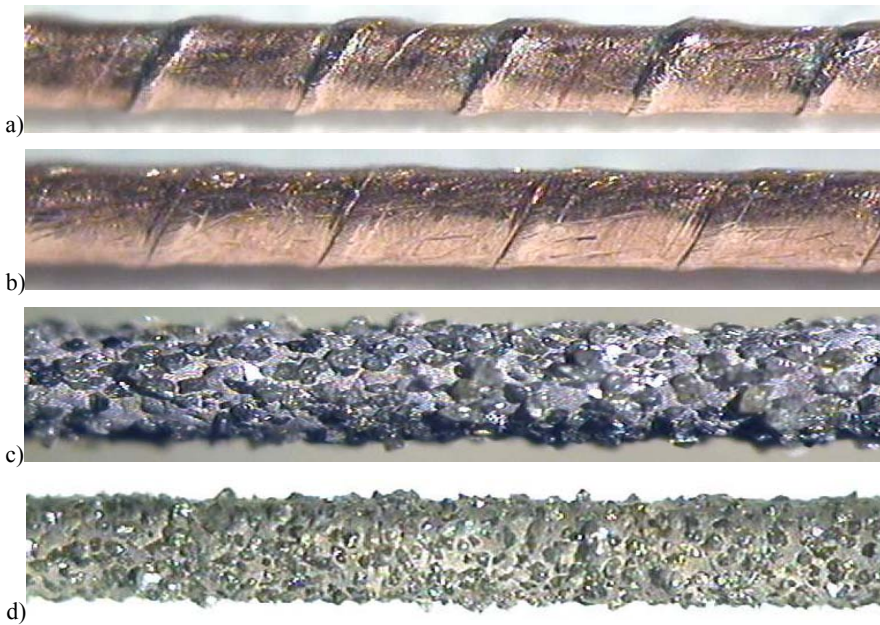
Fig. 7. Bunch string (7wT0.1WCu0.8p0.6): a) before copper winding is compacted,
b) after compaction by idling, c) after galvanization with diamond grit,
d) after cutting hard ceramics (~2000 mm^2)

As opposed to a core made from tungsten wires, a core made from aramid fibres does not need to be coated before copper strip is wound around it. In our experience,

aramid strings (which can be called hybrid strings) are so far the best bunch-string tools. They are characterized by great cross-sectional uniformity and high abrasive endurance.

3. Conclusions

Different bunch-string designs have been presented. Cores made from tungsten wires or aramid fibres have proved to be the best. Cores made from glass or carbonized fibres are too fragile, regardless of the binder used.

The best tungsten or aramid bunch strings are the ones with rolled copper strip windings, particularly if the latter have overlapping winds and have been compacted by idle running in the cutting machine. Such a winding is an excellent base for a coating of abrasive diamond grit dispersed in a nickel binder.

Copper windings can also be put on cores made from aramid fibres bound with a polymer binder. The durability and cutting performance of the bunch strings obtained in this way are comparable with those of the tungsten wire bunch strings.

References

[1] Ciałkowska B. et al.: *Forming Hard Materials by Cutting with Modern String Tools* (in Polish), Report No 4/2001 ITMiA, Wrocław University of Technology, Series REPORTS No 4/2001, Wrocław 2001.
[2] Ciałkowska B., Kośmider J.: *Narzędzie tnące w postaci pętli, nawiniętej z drutów lub włókien, tworzących wiązkę równoległą*, Zgłoszenie patentowe Nr 9/Z/99, Wrocław 1999.
[3] Ciałkowska B., Szymkowski J.: *Sposób wytwarzania pętli bez końca z wiązki równoległej drutów lub włókien oraz urządzenie do wytwarzania pętli bez końca z wiązki równoległej drutów lub włókien*, Zgłoszenie patentowe Nr 10/Z/99, Wrocław 1999.
[4] Ciałkowska B.: *Wydajność przecinania wybranych materiałów strunami wiązkowymi*. Automatyzacja Produkcji 2000, Wiedza – Technika – Postęp, Wrocław, 7–8 grudzień 2000.
[5] Ciałkowska B.: *Przecinanie strunowe materiałów kompozytowych z osnową polimerową zbrojonych włóknami szklanymi, karbonizowanymi i kewlarowymi*, XXIII Naukowa Szkoła Obróbki Ściernej, Rzeszów–Myczkowce, 14–16 wrzesień 2000.

**Wpływ budowy wiązkowych narzędzi strunowych
na ich trwałość podczas cięcia ceramiki technicznej**

Przedstawiono niektóre z wyników badań nad wpływem budowy struny wiązkowej w postaci pętli na jej trwałość w czasie przecinania ceramiki technicznej. Struna wiązkowa zużywa się w miejscach o powiększonej średnicy w wyniku przetarcia i zerwania oplotu. Badania tak prowadzono, aby uniknąć przetarcia i zerwania oplotu. W tym celu stosowano oploty wiązki z różnych materiałów, o różnej średnicy i zmiennym skoku. Rdzenie wykonano

z drutu stalowego 0H18N9 o średnicy ϕ 0,1 mm oraz drutu wolframowego ϕ 0,1 mm z różną liczbą drutów w wiązce (od 7 do 19). Na rdzenie wiązkowe stosowano oplot z różnych materiałów o różnej średnicy (drut stalowy ϕ 0,1 mm, drut wolframowy ϕ 0,07 mm, włókno szklane, kewlarowe i żyłką poliamidową ϕ 0,16 mm) o zmiennym skoku (od 0,1 do 0,6 mm). Określono wpływ skoku oplotu na trwałość struny. Szczególną uwagę zwrócono na następujące dwa czynniki decydujące o trwałości struny: regularny, okrągły przekrój struny wzdłuż całej długości pętli oraz jednorodność podkładu pod spoiwo metalowe z nasypem ściernym [1]. Rdzenie wiązkowe narzędzi strunowych i oploty o zmiennym skoku wykonywano na specjalnie skonstruowanym do tego celu stanowisku, które zostało zgłoszone do ochrony patentowej [2, 3]. Badania mikroskopowe prowadzono na stanowisku ze specjalnym oprzyrządowaniem wyposażonym w mikroskop stereoskopowy Nikon z torem wizyjnym wraz z komputerem.

Identification of linear and non-linear systems with Walsh wavelet packets

W. GLABISZ

Wrocław University of Technology, Wybrzeże Wyspiańskiego 27, 50–370 Wrocław

An algorithm for the identification of the parameters of models, based on the least-squares method and exploiting the properties of the signal wavelet packet analysis, has been proposed. A short introduction to wavelet and wavelet packets' analysis was presented. It has been shown that the *n*-th step of the Walsh wavelet packet analysis can yield filtered, smooth forms of the deterministic or randomly disturbed signal and its derivatives, which generally enable the identification of the model parameters being sought. Multipliers needed to determine the actual, discrete values of the signal function and its derivatives have been formulated. The proposed approach to the identification of model parameters has been validated for linear and nonlinear differential equations of the first to fourth order inclusive. It was stated that the Walsh wavelet packet analysis is an efficient and numerically effective tool in parameters identification process of complicated nonlinear problems of mechanics.

Keywords: *identification, wavelet analysis, Walsh basis*

1. Introduction

One of the primary tasks of modern mechanics is the identification of mathematical models of real systems. This is usually done through a sequence of measurements of, e.g., the excitation and displacement of the system being investigated. Because of the wide spectrum of the problems involved and the diversity of the methods applied, there are many different classifications of identification in a broad sense. One of them is based on the space in which a description of the system to be identified is sought. Accordingly, identification is divided into parametric identification and nonparametric identification. Parametric identification consists in searching for solutions in a parameter base and determining their values in the adopted mathematical model of the system to be identified. Nonparametric identification consists in searching for solutions in a function base and finding the best functional representation of the variation of the quantities characterizing the system to be identified without adopting a mathematical model of the latter.

Basic parametric identification methods [1] include:

• the prediction-error identification approach (PEM) which contains well-known procedures, such as the least-squares (LS) method, the maximum-likelihood (ML)

method, Bayasian maximum a posteriori (MAP) estimation and Akaike's information criterion (AIC),

• the correlation approach which contains the instrumental-variable (IV) technique, as well as several methods for rational transfer functions models.

A critical review of most of the above methods and an attempt at their assessment can be found in [2].

Recently, wavelet analysis [3–5] has been applied to the identification of linear and non-linear systems. In such applications, a solution to a problem is sought by expanding the assumed forms of mathematical models in wavelet bases [6–7].

An important numerical problem of parametric identification is the determination of derivatives of the signal measured, particularly if the measurements (of, e.g., the displacement of a structural point) are randomly disturbed and contain errors and the mathematical model adopted has the form of a differential equation which includes high derivatives of the quantity measured [8].

The aim of the paper is to demonstrate the effectiveness of the Walsh wavelet packet analysis [3] in the search for good representations of signal derivatives which are then used to identify parameters by means of the least-squares (LS) procedure.

In chapter 2, one can find a brief introduction to wavelet analysis and signal wavelet packet analysis; an algorithm for determining signal derivatives on the basis of wavelet expansions in the Walsh wavelet packet analysis is presented in chapter 3; the numerical test results obtained using the proposed approach are presented in chapter 4, and conclusions are drawn in chapter 5.

2. Short introduction to wavelet and wavelet packet analysis of signal

Wavelets $\psi(t)$, as the name suggests, are "small waves" having a limited range and oscillatory character. The word *function* is often omitted in the definition of wavelets since in most cases there is no analytical notation for them and their values are determined recurrently in a finite set of points. Wavelets make up peculiar sets of base functions in a description of discrete and irregular functions (signals) found in the response to mainly real physical systems, particularly chaotic systems. As opposed to the Fourier base, whose elements are simple trigonometric functions with an infinite range, wavelets with their limited range and generally fast disappearance make up bases well located in time t. The Fourier base functions are perfectly located in the domain of frequency and so they constitute an excellent base for stationary and periodic functions in the description of which it is not necessary to locate harmonic components in time. This is simply due to the unlimited range of base functions. The latter cannot be located in time and consequently, this type of analysis in the description of non-stationary phenomena usually leads to a large set of approximation functions. As opposed to the Fourier bases, the bases of wavelet functions are well located in both frequency and time domains. Wavelet function bases are formed by scaling (by parameter a) and shifting in time (by parameter b) initial wavelet (mother wavelet)

$\psi(at+b)$, which leads to the so-called scalable, hierarchical representation of a considered function or signal.

We can consider a signal as consisting of smooth basic part ($f_j(t)$), constituting the core of a description, and part ($d_j(t)$) which contains information about the usually small fluctuations (details) of the signal. This approach allows one to view a signal from the perspective of the adopted scale setting a limit for perceiving details. By adopting a perception scale details, which can be "perceived" in the signal only at lower scales, are neglected in its description. This means that a more accurate description of a signal (a description at a higher resolution $j + 1$ $f_{j+1}(t)$) will be obtained if details $d_j(t)$, which a scale defined as $1/2^j$ permit to be perceived, are added to its lower-resolution (j) ($f_j(t)$) description [3]. This fact can be represented as

$$f_{j+1}(t) = f_j(t) + d_j(t) . \tag{1}$$

By reducing the scale further, an increasingly more accurate description of the signal analyzed is obtained and the procedure close to zero yields a full description of the signal, which can be represented as

$$f(t) = f_j(t) + \sum_{k=j}^{\infty} d_k(t) . \tag{2}$$

This approach to the description of the function spaces of square-integrable functions ($f(t) \in L^2(R)$) can be interpreted as a search for a description of them in space V_j ($f(t) \in V_j$), supplemented with the details of the description in spaces $\{W_k\}$ ($d_j(t) \in W_j$). Formally, $f_j(t)$ is projection f on space V_j. If V_{j+1} denotes space V_j supplemented with space W_j, a description of this fact assumes the following form

$$V_{j+1} = V_j \oplus W_j \tag{3}$$

and it can be interpreted as the decomposition of space V_{j+1} into spaces V_j and W_j which are mutually orthogonal ($W_j \perp V_j$). The decomposition can be continued further (e.g. down to level J) in accordance with this formula

$$V_{j+1} = W_j \oplus V_j = W_j \oplus W_{j-1} \oplus V_{j-1} = ... = W_j \oplus W_{j-1} \oplus ... \oplus W_{j-J} \oplus V_{j-J} , \tag{4}$$

where $W_j \perp W_k$ $(j \neq k)$ and $W_j \perp V_k$ $(j > k)$. If decomposition procedure (4) is continued further, then at the limit transition we get $\lim\limits_{j \to -\infty} V_j = \{0\}$ on one side and $\lim\limits_{j \to \infty} V_j = L^2(R)$ on the other side.

If $f(t) \in V_0$ (sometimes referred to as a central space), then shifts k of function f, $f(t-k) \in V_0$, which shows that space V_0 and the other spaces (V_j, $j \neq 0$) are invariant because of translation. If $f(t) \in V_j$, then at this approximation level $f(t)$ does not include fluctuations (details) perceivable at scales lower than $1/2^j$ and its rescaled form $f(2t)$ does not include details perceivable at scales below $1/2^{j+1}$. This means that $f(2t) \in V_{j+1}$. If it is assumed that function $\phi(t)$ (the so-called scaling function), whose translations generate an orthonormal base of central space V_0, exists in this space, then under the above conditions, functions $\phi_{jk} = 2^{j/2} \phi(2^j t - k)$ form an orthonormal base of space V_j.

The above conditions, together with scaling function $\phi(t)$, define the so-called multiresolution analysis, which enables the representation of spaces and, consequently, the representation of the signals (functions) which the spaces include.

Only functions which fulfill the above conditions can constitute bases of space V_j and (after transformations) bases of their orthogonal supplements W_j. Scaling function $\phi(t)$ and the functions resulting from its shifts k form base $\{\phi_{jk}(t)\}$ of space V_j, where $\phi_{jk} = 2^{j/2} \phi(2^j t - k)$. As we know $V_0 \subset V_1$, hence each function in V_0 can be represented by a base of space V_1. In particular, scaling function $\phi(t) \in V_0$ can be expressed in base $\{\phi_{1k}(t)\}$

$$\phi(t) = \sum_k h_k \phi_{1k}(t) = \sqrt{2} \sum_k h_k \phi(2t - k) . \tag{5}$$

Equation (5) is called a dilation equation and set of expansion coefficients $\{h_k\}$ is referred to as a low-pass filter.

Space W_0 constitutes an orthogonal supplement to space V_0 which as a result becomes space V_1

$$V_1 = V_0 \oplus W_0 \tag{6}$$

and so, since wavelet $\psi(t-k) \in W_0$ and $W_0 \subset V_1$, one can represent $\psi(t)$ as a super-position of base functions in space V_1

$$\psi(t) = \sum_k g_k \phi_{1k}(t) = \sqrt{2} \sum_k g_k \phi(2t - k), \tag{7}$$

where set of coefficients $\{g_k\}$ is called a high-pass filter. Equation (7) is called a wavelet equation. The scaled versions of function $\psi(t)$ constitute bases of space $W_j : \{\psi_{jk}(t) = 2^{j/2} \psi(2^j t - k)\}$. Equations (5) and (7) are referred to as two-scale relations.

The discrete wavelet transform of $f(t)$ can be shown as the decomposition

$$f(t) = \sum_k f_k^j \phi_{jk}(t) + \sum_{l=j}^{\infty} \sum_k d_k^l \psi_{lk}(t), \tag{8}$$

where $f_k^j = \langle \phi_{jk}, f \rangle$ and $d_k^j = \langle \psi_{jk}, f \rangle$. For the scale parameter in the form $a = 2^{-j}$, the hierarchical wavelet decomposition (8) produces signal components whose spectra form the so-called consecutive octave bands. In certain application, the wavelet decomposition may not be fine enough to meet the problem requirements. To solve this problem we may use continuous wavelet transform substituting a smaller increment for the scale parameter a or we may apply wavelet packets which are used in this article.

A wavelet packet is a generalization of a wavelet in that each octave frequency band of the wavelet spectrum is further subdivided into finer frequency bands by using the two-scale relations repeatedly. The space V can be decomposed into a direct sum of two orthogonal subspaces defined by their basis functions given by (5) and (7). This splitting algorithm can be used to decompose W spaces as well. For example, if we define

$$w_2(t) = \sqrt{2} \sum_k h_k \psi(2t - k),$$
$$w_3(t) = \sqrt{2} \sum_k g_k \psi(2t - k), \tag{9}$$

then $\{w_2(t-k)\}$ and $\{w_3(t-k)\}$ are orthonormal basis functions for the two subspaces whose direct sum is W_1.

In general, for $n = 0, 1, \ldots$ we define a sequence of functions

$$w_{2n}(t) = \sqrt{2}\sum_k h_k w_n(2t - k),$$

$$w_{2n+1}(t) = \sqrt{2}\sum_k g_k w_n(2t - k). \tag{10}$$

$w_{0,3}$							
$w_{0,2}$				$w_{1,2}$			
$w_{0,1}$		$w_{1,1}$		$w_{2,1}$		$w_{3,1}$	
$w_{0,0}$	$w_{1,0}$	$w_{2,0}$	$w_{3,0}$	$w_{4,0}$	$w_{5,0}$	$w_{6,0}$	$w_{7,0}$
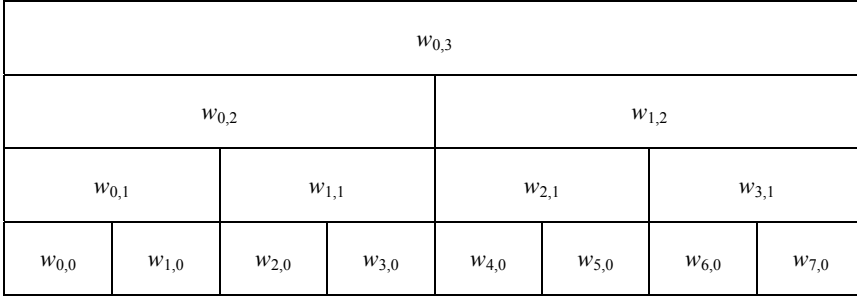
Fig. 1. The decomposition diagram of the space $w_{0,3}$ (V_3) using wavelet packets
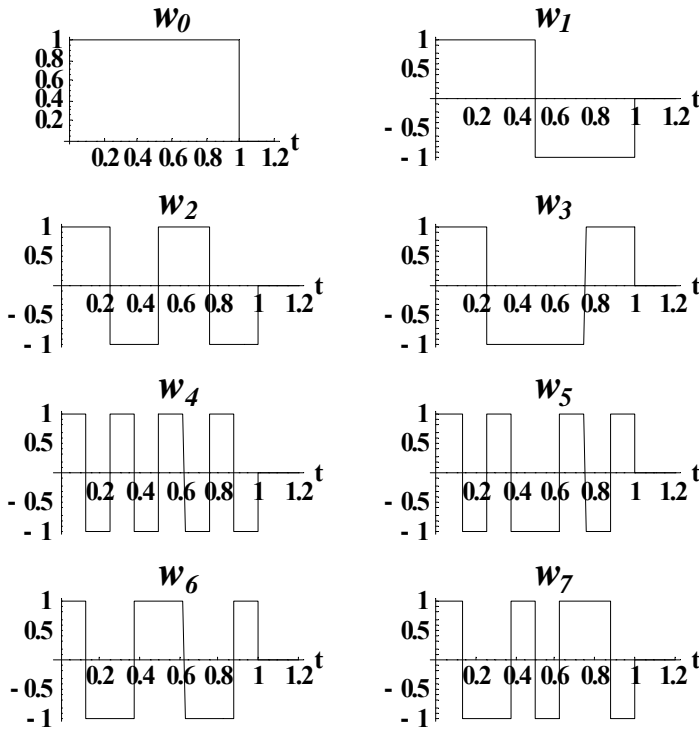
Fig. 2. Exemplary Walsh wavelet basis function

So far we have been using the combination of $\left\{\phi\left(2^{j}t-k\right)\right\}$ and $\left\{\psi\left(2^{j}t-k\right)\right\}$ to form a basis for V_J, and now we have a whole sequence of $w_n(t)$ at our disposal. Various combinations of these and their dilations and translations can give rise to various bases for the function space. We have a whole collection of orthonormal bases generated from $\left\{w_n(t)\right\}$ which is called a "library of wavelet packet bases". The function of the form $w_{njk} = 2^{j/2}w_n\left(2^{j}t-k\right)$ is called a wavelet packet. In Figure 1 the diagram, which illustrates the decomposition of the space $w_{0,3}$ (V_3) using wavelet packets, is shown.

The Haar basis exploited in that article is obtained with a multiresolution of piecewise constant function. The low-pass $\left\{h_k\right\}$ and high-pass $\left\{g_k\right\}$ filters have only two non-zero coefficients $h_0 = h_1 = 1/\sqrt{2}$ and $g_0 = -g_1 = 1/\sqrt{2}$, respectively. The Haar wavelet has the shortest support among all orthogonal wavelets. It has only one vanishing moment so it is not well adopted to approximating smooth functions.

In the wavelet packet analysis, Haar filters generate the so-called Walsh wavelet packets. The Walsh wavelet packets are the Walsh functions – square waves oscillating over a compact support. Figure 2 presents exemplary Walsh wavelet packets for the bottom-most raw of space decomposition shown in Figure 1.

3. Signal derivatives in the Walsh wavelet packet analysis

Let us assume that the available physical quantity measured is, e.g., displacement or rotation. As a rule, there is sequence N of numbers describing a physical quantity varying through signal duration t. Let us further assume that measurements are taken at a constant sampling period. Searching for a mathematical model, which would describe a physical quantity measured, we usually assume that the model belongs to a selected class of mathematical descriptions with unknown coefficients which are sought in the course of its identification. Generally, the description has the form of a differential equation or equations of a given order. It is assumed here that it is one linear or non-linear ordinary differential equation with coefficients constant in time. A mathematical model of this kind has often been successfully used to describe mechanical systems, and not only simple ones [9]. Depending on the assumed order of the differential equation, we usually have to determine a series of derivatives of the signal measured. Wavelet packet analysis based on the Haar filter has been found to be particularly useful for the solution of this problem.

The use of the Haar low- and high-pass filters consists in the successive calculation of the weighted sum and the weighted difference, respectively $(a+b)/\sqrt{2}$ and $(a-b)/\sqrt{2}$, for pairs of numbers (a and b), which follow one another in a sequence of measurements. The application of the low-pass filter to a signal with a number of elements equal to N results in the weighted averaging of the signal and the output

product is a size *N*/2 set which is a rescaled, smoothed representation of the input signal. Because during measurement also small (by assumption), random disturbances are recorded and the measurement itself is recorded with an error, it is desirable to eliminate the above factors and filtering the signal through the low-pass filter does this. By applying the Haar high-pass filter to a size *N* sample, one obtains a set (size *N*/2) of rescaled differences between pairs of numbers, which is an derivative representation of input signal exact to the sign, the sampling rate and the scale introduced by the filter. The application of the Haar high-pass filter consists in the differential calculation of the scaled signal derivative. If the set representing the scaled input signal derivative is resubjected to filtration by means of the Haar high-pass filter, a size *N*/4 set (twice smaller than the input set) representing the scaled second derivative of the signal originally subjected to filtration will be obtained. The Walsh wavelet packet analysis algorithm can perform, among others, such repeated filtration. Thus, once proper multipliers for scaling are found, the result of the Walsh wavelet packet analysis can be used directly as the source of the input signal and its differentially calculated derivatives of the order required by the adopted model.

$s_{0,0}$															
$C^0(1)s_{1,0}$								$C^1(1)s_{1,1}$							
$C^0(2)s_{2,0}$				$C^1(2)s_{2,1}$								$C^2(2)s_{2,3}$			
$C^0(3)s_{3,0}$		$C^1(3)s_{3,1}$				$C^2(3)s_{3,3}$								$C^3(3)s_{3,7}$	
$C^0(4)*$ $s_{4,0}$	$C^1(4)*$ $s_{4,1}$		$C^2(4)*$ $s_{4,3}$				$C^3(4)*$ $s_{4,7}$								$C^4(4)*$ $s_{4,15}$

Fig. 3. Packet analysis algorithm chart

The packet analysis algorithm chart is shown in Figure 3. The top row in the chart represents input signal $s_{0,0}$ which is subjected to successive *n* steps of filtration in the packet analysis procedure. Signal $s_{0,0}$ has not been filtrated before and so it is assigned $n = 0$. The successive filtration steps yield blocks of coefficients $s_{i,j}$, equal in size, for fixed *n*. The coefficients in Figure 3 have been multiplied by multipliers $C^p(n)$, where $p \geq 0$ denotes the order of the signal derivative. The products of the packet expansion coefficients and the multipliers are: at $p = 0$, ($C^0(n)s_{i,j}$) – the fil-

tered input signal, at $p = 1$, ($C^1(n)s_{i,j}$) – the first derivative of the filtered input signal and at $p = 2$, ($C^2(n)s_{i,j}$) – the second derivative of the signal. Multipliers $C^p(n)$, depend on filtration step n, the Haar filter coefficients, size N of the set which describes the input signal, signal sampling rate $\Delta = t / N$ and order p of the sought signal derivative. In Figure 3, only four filtration steps are shown and one can easily see that the signal expansion coefficients in the last step ($s_{4,j}$) can be a basis for reproducing the filtered input signal ($C^0(4)s_{4,0}$) and its first ($C^1(4)s_{4,1}$), second ($C^2(4)s_{4,3}$), third ($C^3(4)s_{4,7}$) and fourth ($C^4(4)s_{4,15}$) filtered derivative. The maximum order (p) of the derivative, which can be reproduced at step n of the wavelet packet analysis, is $p = n$. One can notice that signal derivatives can be reproduced also from other blocks of signal expansion coefficients at the n-th level of signal filtration.

Furthermore, only the multipliers necessary to identify the signal and its derivatives for their first (from the chart's left side) representations at the level n are given. Multipliers $C^p(n)$ can be easily determined by monitoring the sequence of signal filtration whose idea is presented above. The filtered signal representation occurs always as the first block of coefficients (a size $N / 2^n$ sequence of numbers) in the signal expansion at step n of the signal packet analysis. Multiplier $C^0(n)$ has this form:

$$C^0(n) = \left(\frac{1}{\sqrt{2}}\right)^n . \tag{11}$$

The filtered representations of the first, second, third and fourth signal derivative occur at respective positions 2, 4, 8 and 16 of level n (starting from its left). Each of the sets has size $N / 2^n$. The multipliers for the derivatives are respectively:

$$
\begin{aligned}
C^1(n) &= (-1)\cdot 4 \cdot (2^n \Delta)^{-1} \cdot (1/\sqrt{2})^n, \\
C^2(n) &= (-1)^2 \cdot 32 \cdot (2^n \Delta)^{-2} \cdot (1/\sqrt{2})^n, \\
C^3(n) &= (-1)^3 \cdot 512 \cdot (2^n \Delta)^{-3} \cdot (1/\sqrt{2})^n, \\
C^4(n) &= (-1)^4 \cdot 16384 \cdot (2^n \Delta)^{-4} \cdot (1/\sqrt{2})^n.
\end{aligned}
\tag{12}
$$

Generally, multiplier $C^p(n)$ of the p-th order derivative (assuming that $p \le n$) is:

$$C^p(n) = \left(\frac{1}{\sqrt{2}}\right)^n \prod_{i=1}^{i=p} (-1)\cdot 4 \cdot 2^{(i-1)} \cdot (2^n \Delta)^{-1} . \tag{13}$$

The first (if the blocks of packet expansion elements for level n are counted from the left) rescaled representation of the signal derivative of order p occurs at position 2^p. One can easily check if the multipliers expressed by relations (11) and (13) are correct by carrying out a Walsh wavelet packet analysis of discrete representations of the smooth functions whose derivatives are known.

4. Numerical examples

The possibility of applying the results of the Walsh wavelet packet analysis to the identification of simple models of mechanical systems was tested for several cases. As mentioned above, the least-squares method [1,10] was used to identify the coefficients of the mathematical models assumed.

The first case considered is the identification of the coefficients of a second-order differential equation which can be used to describe, for example, 1DOF system vibrations. The identification is based on known, undisturbed sequences of numbers obtained by sampling the system response and excitation at a constant rate. Let us assume that the mathematical description being sought has this form

$$ay''(t) + by'(t) + cy(t) = f(t), \tag{14}$$

where a, b, c are the constant parameters being sought and $y(t)$ and $f(t)$ are functions described by sequences of numbers y_i and f_i formed as a result of the sampling of, e.g., deflection and excitation. The discrete values of the first and second derivatives of signal $y(t)$ are denoted by, respectively, $y_t'(t)$ and $y_t''(t)$, where $i = 1,2,3,...,N$. The results of the identification of equation (14) at $a = 2$, $b = 0.1$, $c = 5$ and $f = 11\cos(t)$ for the signal packet analysis step n being a source of equal-size (size l) sets, which describe discretely $y(t)$, $y'(t)$ and $y''(t)$, are presented as parameter values and their calculation errors are compared with the exact values in Tables 1 and 2. The results are based on respectively size $N = 16384$ sets and size $N = 32768$ sets describing system response $y_i = y(t_i)$ and excitation $f_i = 11\cos(t_i)$ for $t \in [0,10]$. It becomes evident that the model parameters can be determined with an error of below 8% already on the basis of $4\times8 = 32$ numbers, 24 of which are appropriate signal packet expansion coefficients and the other 8 numbers are excitation measurements. If $4\times32 = 128$ numbers are used in the identification, the percentage error of the coefficients being determined does not exceed 0.5%

The second considered case of the application of the Walsh wavelet packet analysis is the identification of the coefficients of the non-linear model which is often used to represent the problem of vibration of systems exhibiting chaotic motion features [11]. The mathematical model assumes here the form of the Duffing equation:

$$ay''(t) + by'(t) + cy^3(t) = f(t).$$ (15)

Table 1. Identification results of the linear 1DOF system (14) for $N = 16384$

Stage n of wave-let packet analysis	Number of ele-ments l	Parameters (exactly: $a = 2$, $b = 0.1$, $c = 5$)					
		a		b		c	
		Estimation	% Error	Estimation	% Error	Estimation	% Error
5	512	1.9999	−0.0046	0.1001	0.1349	5.0000	0.0007
7	128	1.9993	−0.0324	0.1001	0.1529	5.0005	0.0100
9	32	1.9902	−0.4862	0.1003	0.3901	5.0057	0.1531
11	8	1.8417	−7.9114	0.1042	4.2850	5.1245	2.4904

Table 2. Identification results of the linear 1DOF system (14) for $N = 32768$

Stage n of wave-let packet analysis	Number of ele-ments l	Parameters (exactly: $a = 2$, $b = 0.1$, $c = 5$)					
		a		b		c	
		Estimation	% Error	Estimation	% Error	Estimation	% Error
5	1024	1.9999	−0.0011	0.1000	0.0752	5.0000	0.0005
7	256	1.9998	−0.0087	0.1000	0.0783	5.0000	0.0024
10	32	1.9903	−0.4849	0.1003	0.3306	5.0076	0.1528
11	16	1.9611	−1.9441	0.1010	1.0962	5.0300	0.6139
12	8	1.8418	−7.9095	0.1042	4.2199	5.1245	2.4905

The results of the identification of the model's parameters at $a = 1$, $b = 0.1$, $c = 1$ and $f = 11\cos(t)$ for different rates of sampling the system's response and excitation in time $t \in \langle 0,10 \rangle$ are given in Tables 3 and 4. As one can see, a larger size of sets describing the filtered signal and its filtered derivatives is required than in the case of linear systems. At $l = 64$, the coefficient calculation percentage error is in the order of 1%.

Possible random disturbances in the signal $y(t)$ being measured were generated using a uniform distribution and generate numbers from a $\pm 5\%$ range of the value of amplitude y_i and then adding them to y_i. The parameter identification results for the linear model and the non-linear model, taking into account random signal distur-

bances, are presented respectively in table 5 and 6. As one can see, filtration by the Walsh wavelet packet analysis is sufficient for the identification of model parameters: here at $l = 16$ and $l = 32$ for the linear and non-linear models, respectively.

Table 3. Identification results of the non-linear 1DOF system (15) for $N = 16384$

Stage n of wavelet packet analysis	Number of elements l	Parameters (exactly: $a = 1$, $b = 0.1$, $c = 1$)					
		a		b		c	
		Estimation	% Error	Estimation	% Error	Estimation	% Error
5	512	0.9999	–0.0084	0.1001	0.1179	1.0002	0.0215
7	128	0.9997	–0.0274	0.1004	0.4184	1.0037	0.3721
9	32	0.9956	–0.4346	0.1046	4.6929	1.0598	5.9847
10	16	0.9647	–3.5217	0.0864	–13.518	1.2393	23.932

Table 4. Identification results of the non-linear 1DOF system (15) for $N = 32768$

Stage n of wavelet packet analysis	Number of elements l	Parameters (exactly: $a = 1$, $b = 0.1$, $c = 1$)					
		a		b		c	
		Estimation	% Error	Estimation	% Error	Estimation	% Error
5	1024	0.9999	–0.0039	0.1000	0.0590	1.0000	0.0049
7	256	0.9999	–0.0085	0.1001	0.1384	1.0009	0.0926
9	64	0.9991	–0.0893	0.1012	1.2984	1.0149	1.4946
10	32	0.9956	–0.4307	0.1046	4.6435	1.0598	5.9855
11	16	0.9648	–3.5174	0.0864	–13.557	1.2393	23.932

In the above cases, the parameters of low (second)-order equations were identified. Let us assume now that we look for a mathematical description of the measured quantities (y_i, f_i) in a class of fourth-order differential equations. Let the exemplary equations, whose constant coefficients are sought, have the form:

$$ay''''(t) + by'''(t) + cy''(t) + dy'(t) + ey(t) = f(t), \tag{16}$$

$$ay''''(t) + by'''(t) + cy''(t) + dy'(t) + ey^3(t) = f(t),\tag{17}$$

respectively, for the linear and non-linear problem.

Table 5. Identification results of the linear 1DOF system (14) with random disturbance for $N = 16384$

Stage n of wave-let packet analysis	Number of ele-ments l	Parameters (exactly: $a = 2$, $b = 0.1$, $c = 5$)					
		a		b		c	
		Estimation	% Error	Estimation	% Error	Estimation	% Error
9	32	1.4505	–27.472	0.1938	93.859	4.0966	–18.068
10	16	1.9267	–3.6619	0.0984	–1.5231	4.9983	–0.0333
11	8	1.8297	–8.5112	0.1144	14.453	5.0917	1.8347

Table 6. Identification results of the non-linear 1DOF system (15) with random disturbance for $N = 16384$

Stage n of wave-let packet analysis	Number of ele-ments l	Parameters (exactly: $a = 1$, $b = 0.1$, $c = 1$)					
		a		b		c	
		Estimation	% Error	Estimation	% Error	Estimation	% Error
8	64	0.5577	–44.224	0.0530	–46.949	0.6874	–31.257
9	32	1.0033	0.3313	0.0960	–3.9761	1.0802	8.0219
10	16	0.9661	–3.3852	0.0844	–15.555	1.2462	24.626

The results of the identification of the equations' parameters for different steps n of the packet analysis of the signal of size $N = 16384$ are given in Tables 7 and 8 for respectively linear model (16) and non-linear model (17) at $f(t) = 11\cos(t)$.

Since the determination of high derivatives of the measured signal is very laborious and generally yields poor results [8], it is often eliminated in various ways. By carrying out the Walsh wavelet packet analysis of the signal one can obtain acceptable forms of its high derivatives, which – as Tables 7 and 8 show – can be used to identify successfully model parameters.

Table 7. Identification results of the linear system (16) for $N = 16384$

Stage n of wavelet packet analysis	Number of elements l	Parameters (exactly: $a = 30$, $b = 8$, $c = 15$, $d = 6$, $e = 2$)									
		a		b		c		d		e	
		Estimation	% Error	Estimation	% Error	Estimation	% Error	Estimation	% Error	Estimation	% Error
9	32	28.760	−4.132	8.515	6.439	13.197	−12.013	6.446	7.437	1.470	−26.481
10	16	30.258	0.862	7.876	−1.537	15.297	1.985	5.891	−1.806	2.078	3.921
11	8	30.631	2.105	8.104	1.300	15.256	1.711	6.126	2.116	2.046	2.344

Table 8. Identification results of the non-linear system (17) for $N = 16384$

Stage n of wavelet packet analysis	Number of elements l	Parameters (exactly: $a = 30$, $b = 8$, $c = 15$, $d = 6$, $e = 2$)									
		a		b		c		d		e	
		Estimation	% Error	Estimation	% Error	Estimation	% Error	Estimation	% Error	Estimation	% Error
8	64	27.228	−9.238	9.238	18.610	12.300	−18.000	6.367	6.124	1.881	−5.932
9	32	30.022	0.074	7.288	−8.894	15.361	2.412	5.580	−6.990	1.993	−0.345
10	16	30.883	2.943	6.644	−16.945	15.967	6.451	5.395	−10.070	2.061	3.056

5. Concluding remarks

An algorithm for the identification of the parameters of models (in the form of differential equations) based on the least-squares method and exploiting the properties of the signal wavelet packet analysis has been presented. It has been shown that the n-th step of the Walsh wavelet packet analysis can yield filtered, smooth forms of the signal and its derivatives, which generally enable the identification of the model parameters being sought. Multipliers required to determine the actual, discrete values of the signal function and its derivatives have been formulated. The approach to the identification of model parameters has been validated for linear and non-linear differential equations of the first to fourth order, inclusive.

From the test results several general conclusions can be drawn:

- owing to the properties of the Haar filters, the Welsh wavelet packet analysis is a natural source of signal derivatives needed for the identification of model parameters;
- the forms of the scaled function and its derivatives obtained at the n-th step of the packet analysis are represented by equal-size, discrete sets of wavelet expansion coefficients, from which most measuring errors and random disturbances (having an adverse effect on model parameter identification) of measured input quantities have been eliminated by filtration;
- unlike other wavelet filters, the Haar filter's low- and high-pass forms make it possible to formulate exact multipliers for the rescaled function and its derivatives without introducing any boundary disturbances;
- at each (appropriately high) step n of the packet analysis one can find repeatedly occurring representations of a signal derivative of a given order; in the reproduction of the actual form of the derivative, the representations are equivalent;
- in the identification of models, particularly the ones with high-order signal derivatives, special attention must be paid to the selection of packet analysis step n whose coefficients are the basis for the reproduction of the signal and its derivatives.

References

[1] Ljung L.: *System Identification: Theory for the User*, Prentice Hall PTR, New Jersey, 1987.
[2] Petsounis K., Fassois S.D.: *Parametric time-domain methods for the identification of vibrating structures – A critical comparisons and assessment*, J. Mechanical Systems and Signal Procesing, Vol. 15, No. 6, 2001, 1031–1060.
[3] Mallat S.: *A Wavelet Tour of Signal Processing*, Academic Press, London, 1998.
[4] Resnikoff H.L., Wells R.O.Jr.: *Wavelet Analysis. The Scalable Structure of Information,* Springer-Verlag, New York, 1998.
[5] Percival D.B., Walden A.T.: *Wavelet Methods for Time Series Analysis*, Cambridge University Press, Cambridge, 2000.
[6] Ghanem R., Romeo F.: *A wavelet-based approach for the identification of linear time-varying dynamical systems*, J. Sound and Vibration, Vol. 234, No. 4, 2000, 555–576.

[7] Ghanem R., Romeo F.: J. Non-Linear Mechanics, Vol. 36, 2001, 835–859.

[8] Worden K.: *Data processing and experiment design for the restoring force surface method, Part I: Integration and differentiation of measured time data*, J. Mechanical Systems and Signal Procesing, Vol. 4, No. 4, 1990, 295–319.

[9] Bellomo N., Preziosi L.: *Modelling Mathematical Methods and Scientific Computation*, CRC Press, Boca Raton, 1995.

[10] Chen S., Billings S.A., Luo W.: *Orthogonal least squares methods and their application to non-linear system identification*, Int. J. Control, Vol. 50, No. 5, 1989, 1873–1896.

[11] Argyris J., Faust G., Haase M.: *An Exploration of Chaos*, Elsevier Science, Amsterdam, 1994.

Identyfikacja układów liniowych i nieliniowych z wykorzystaniem pakietowej analizy falkowej z bazą Walsha

W artykule przedstawiono algorytm identyfikacji parametrów modeli, w postaci liniowych i nieliniowych równań różniczkowych, oparty na metodzie najmniejszych kwadratów i wykorzystujący właściwości pakietowej, falkowej analizy sygnału. Przedstawiono podstawy analizy falkowej i pakietowej analizy falkowej. Pokazano, że *n*-ty etap analizy pakietowej z bazą Walsha może być źródłem filtrowanych, wygładzonych postaci deterministycznego bądź losowo zakłóconego sygnału i jego pochodnych, które na ogół z powodzeniem pozwalają identyfikować poszukiwane parametry modelu. Sformułowano mnożniki, które są niezbędne do określania rzeczywistych, dyskretnych wartości funkcji i jej pochodnych. Zaproponowane podejście do identyfikacji parametrów modelu testowano na liniowych i nieliniowych równaniach różniczkowych do rzędu czwartego włącznie. Stwierdzono, że pakietowa analiza falkowa z bazą Walsha może być skutecznym i numerycznie efektywnym narzędziem w procesie identyfikacji parametrycznej złożonych nieliniowych modeli zagadnień mechaniki.

Possibility of controlling the final stress
in the surface layer after grinding

J. HARASYMOWICZ, A. MIERNIKIEWICZ, L. PRZYBYLSKI

Kraków University of Technology, Al. Jana Pawła II 37, 31-864 Kraków

The investigations, which indicate the possibility of controlling the final stresses residing in the surface layer after grinding of a shaft hardened steel being toughened to 56 HRC, have been presented. The results obtained indicate that it is possible to forecast the maximum value of the final stress in the surface layer by an appropriate selection of the machining parameters. The measurement method, adopted by Sachs and Espey, has been applied in determining the final stress in the surface layer. The method consists in the measurement of the diameter change of a ring cut through after grinding and removal of its surface layer using stress-free way, i.e. electrolytic etching in a special device. The obtained results concerning the influence of the grinding parameters on the value of the final stress have been graphically presented.

Keywords: *grinding, hardened steel, surface layer, final stresses*

1. Introduction

The grinding process causes substantial changes of the thin surface layer (SL) properties. The following phenomena account for these changes:
  1. The plastic deformation taking place as a result of the cutting tool operation.
  2. The heat heterogeneous temperature forming the surface layer.

The changes of the surface layer properties occur mainly as the change of a general hardness and the creation of the final stresses. The depth of this layer is varying within the range from a few microns up to a few tenths of a millimeter, depending upon the material properties and the grinding conditions. The sign and the level of the final stress and the hardness characteristics in the SL are dependent almost exclusively on all conditions of the grinding process [4, 6]. The properly selected grinding conditions can lead to the improvement of all SL features. The improperly selected conditions can cause superficial damage and consequently the part is classified as a reject. The influence of the grinding conditions on SL has not been sufficiently studied from the standpoint of the forecasting needs. The investigation results presented in this paper indicate that it is possible to forecast the maximum value of the final stress in the surface layer by an appropriate selection of the machining parameters.

2. Stress measurements

The measurement method adopted by Sachs and Espey [1, 2] has been applied in determining the final stress in the surface layer; the method consists in change of the shape of the ring cut through after grinding and in removal of the surface layer using stress-free way (electrolytic etching) in a specially designed device [3].

The total peripheral stress σ_t in the ring is represented by the sum of four components:

$$\sigma_t = \sigma_{t1} + \sigma_{t2} + \sigma_{t3} + \sigma_{t4} \ . \tag{1}$$

After cutting through the annular sample the variable component σ_{t1} is calculated as follows:

$$\sigma_{t1} = \frac{E}{1-v^2} \cdot (g - 2x) \cdot \frac{\Delta D_1}{D_m^2} \ , \tag{2}$$

where:

ΔD_1 – change of the diameter after cut,

D_0, D_1 – diameters of the ring middle layers before and after cut,

D_m – mean value of D_0 and D_1,

g – thickness of the ring wall,

E – Young′s modulus of the material sample,

v – the Poisson ratio of the material.

Further the components σ_{t2} and σ_{t3} disappear in a given layer during removing the preceding layers. These components are calculated in the following way:

$$\sigma_{t2} = \frac{1}{g-x} \cdot \int_0^x (\sigma_t - \sigma_{t1}) dx \ , \tag{3}$$

$$\sigma_{t3} = \frac{E}{1-v^2} \cdot (g - x) \cdot \frac{\Delta D}{D_m^2} \ . \tag{4}$$

When we remove the layer determined by the x-coordinate, the following component vanishes:

$$\sigma_{t4} = \frac{E}{1-v^2} \cdot \frac{(g-x)^2}{3D_m^2} \cdot \frac{dD}{dx} \ . \tag{5}$$

The following denotations have been made: $\Delta D = \Delta D' - \Delta D_1$, where:

$\Delta D'$ – the increment of the middle layer after cut through and etching down the depth x,

D – the diameter of the middle layer prior to the removal of the layer determined by the x-coordinate,

dD – the increment of the diameter of the middle layer caused by the removal of a layer of material determined by the x-coordinate.
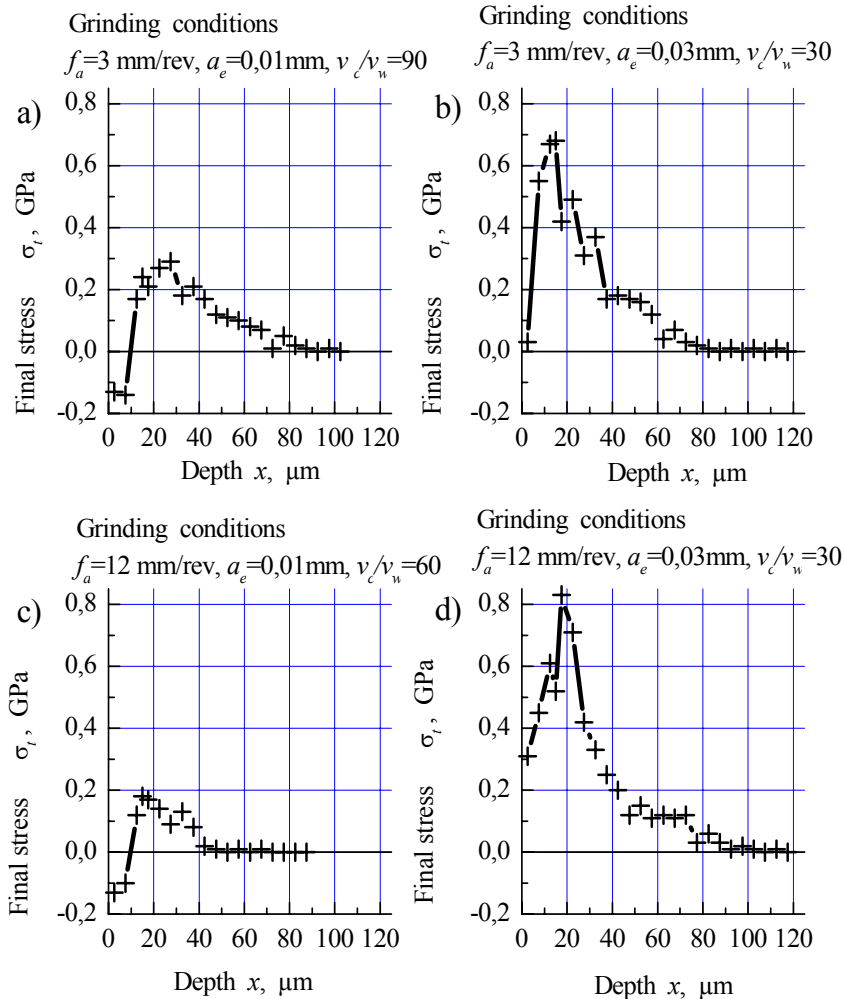
Fig. 1a, b, c, d. Examples of the occurrence of the final stress σ_t in the surface layer depending upon the applied combinations of parameter variations during the grinding process at the speed $v_c = 50$ m/s

3. The scope of the grinding tests

The experimental investigations have been carried out using a Polish-made grinding machine RUP-28, which enables grinding with the speed v_c up to 60 m/s. The cooling fluid, composed of 5% Hydropol has been applied during grinding. The coolant has been introduced into the grinding area using a regular nozzle, being a part of the standard grinding machine equipment.

The grinding wheels used for tests were sized 500×50×203 mm and denoted as 89A462K5V227/60. The active surface of the grinding wheels has been conditioned, i.e. levelled, cleaned and sharpened by means of a diamond truing tool of "Dianyf" type.

Table 1. The ranges of the grinding conditions applied during tests

Parameter	Denotation	Application range	Unit
Grinding speed	v_c	30÷60	m/s
Ratio of the peripheral wheel speed to the peripheral ring speed	v_c/v_w	30÷90	
Longitudinal feed rate	f_a	3÷12	mm/rev. of piece
Effective grinding depth	a_e	0.01÷0.03	mm

Table 2. Grinding conditions and regression equations to calculate the maximum value of the final stresses

Ratio of speed v_c/v_w	Longitudinal feed f_a mm/rev	Effective grinding depth a_e mm	Material removal V_w mm³	Value of the maximum final stress $\sigma_{t\,max}$ depending on the grinding speed $\sigma_{t\,max} = f(v_c)$
30	3	0.01	1000	$-6.8\cdot10^{-4}\cdot v_c^2+0.0548\cdot v_c-1.312$
30	12	0.03	1000	$-6.88\cdot10^{-4}\cdot v_c^2+0.0796\cdot v_c-1.361$
60	3	0.01	1000	$-4.66\cdot10^{-4}\cdot v_c^2+0.0507\cdot v_c-1.461$
60	12	0.03	1000	$-4.66\cdot10^{-4}\cdot v_c^2+0.0603\cdot v_c-1.311$
90	3	0.01	1000	$-3.38\cdot10^{-4}\cdot v_c^2+0.0493\cdot v_c-1.461$
90	12	0.03	1000	$-3.38\cdot10^{-4}\cdot v_c^2+0.0576\cdot v_c-1.311$

The annular thin-wall samples of NC6 steel (Polish Standard) have been used and their chemical composition was the following: C − 1.4%, Si − 0.92%, Cr − 1.4%. The rings were subjected to the following process prior to be machined:
1. Turning and grinding.
2. Hardening and toughening.
3. Stress relief annealing.
4. Sorting aimed at keeping their hardness within HRC 56 ± 2.

The scope of the parameters applied is presented in the Table 1. The tests have been performed in accordance with the methodology of the experimental investigations [5].
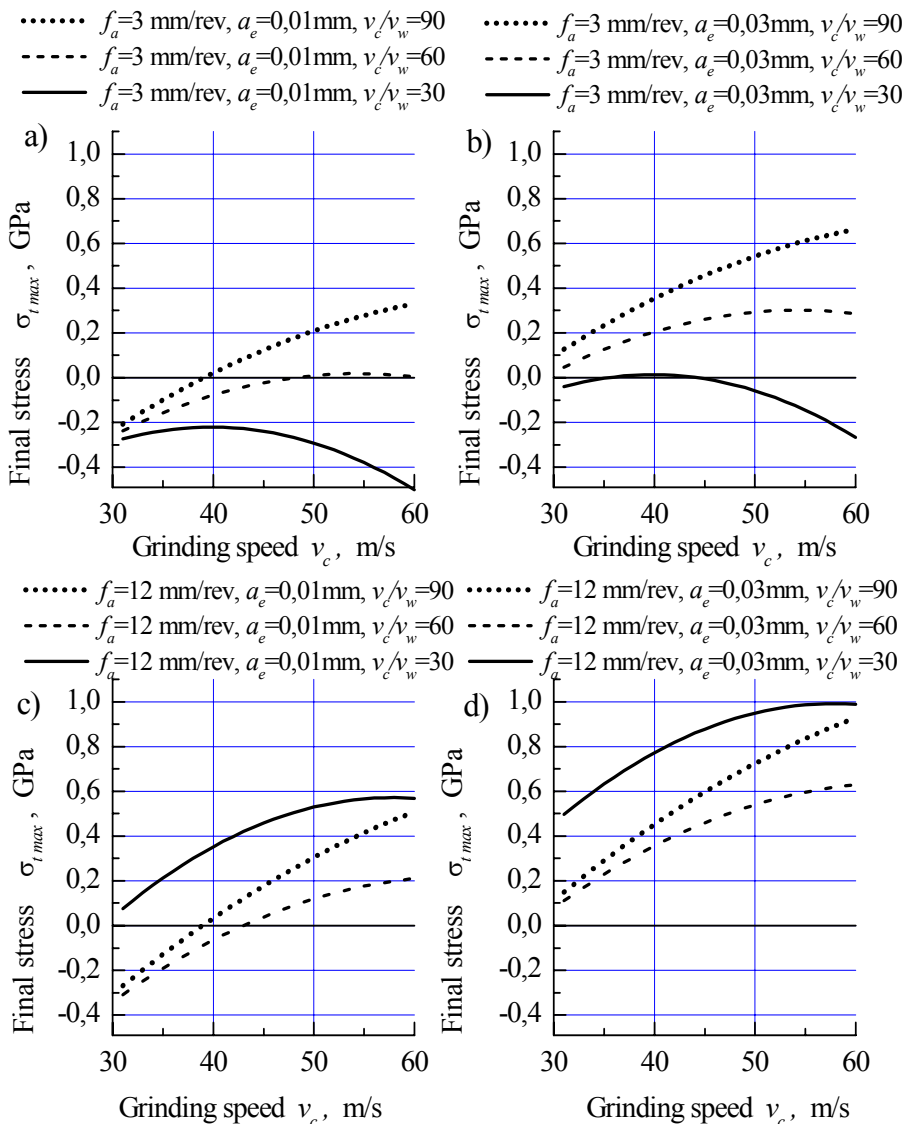
Fig. 2. The occurrence of the maximum final stress $\sigma_{t\,max}$ in the surface layer after grinding

The influence of the grinding speed v_c for various combinations of the grinding depth a_e, the longitudinal feed f_a, and the speed ratios v_c/v_w on the maximum value of the final stress σ_{tmax} is represented by the curves in Figure 1 and Figure 2.

The effect of the applied combination of parameters on the maximum value of the final stress σ_{tmax} is presented as a relationship in Table 2.

4. Conclusions

Based on the research carried out the following conclusions can be drawn:

1. Grinding conditions applied affect considerably the distribution and the value of the final stress in the surface layer of the ground steel.

2. The final stress in the surface layer reaches its maximum values at the depth x ranging from 10 to 20 μm.

3. The maximum value of the final stress in the surface layer after grinding of hardened steel using authorized grinding wheels are predictable, depending upon the grinding conditions being applied.

References

[1] Orłoś Z.: *Pomiary naprężeń w budowie maszyn*, PWT, Warszawa, 1983.
[2] Górecka R., Polański Z.: *Metrologia warstwy wierzchniej*, WNT, Warszawa, 1983.
[3] Przybylski L., Miernikiewicz A., Summer-Brason K.: *Projekt urządzenia do pomiaru naprężeń w warstwie wierzchniej szlifowanych przedmiotów,* Prace ITMiAP Politechniki Krakowskiej, 1978.
[4] Harasymowicz J., Przybylski L.: *Die Restspannungen in der Oberflächenschicht beim Schleifen,* Schleifen und Trennen, Schwaz – Tirol, Austria, Nr 94, 1979, 11–13.
[5] Polański Z.: *Metodyka badań doświadczalnych*, WNT, Warszawa, 1979.
[6] Przybylski L., Miernikiewicz A.: *Badania nad możliwością celowego kształtowania stanu warstwy wierzchniej w procesie szlifowania*, Archiwum Technologii Maszyn, Zeszyt 8, 1990, 477–482.

**Możliwość sterowania wartością naprężeń własnych
w warstwie wierzchniej przedmiotów szlifowanych**

Przedstawiono możliwość sterowania wartością naprężeń własnych w wierzchniej warstwie szlifowanych wałków ze stali ulepszonej do HRC 56±2 przez dobór odpowiednich warunków obróbki.

Celem pracy było wykazanie, że umiejętne sterowanie procesem szlifowania pozwala uzyskać przedmiot obrobiony o zadanych cechach warstwy wierzchniej. Jako próbki do badań użyto cienkościennych pierścieni wykonanych ze stali NC6. Do pomiaru naprężeń w warstwie wierzchniej pierścieni szlifowanych zewnętrznie zastosowano metodę opublikowaną przez Sachsa i Espeya. Wartości naprężeń ostatecznych określono na podstawie wyników pomiarów odkształcenia próbek pierścieniowych. Odkształcenie próbek mierzono w sposób ciągły podczas ich trawienia w specjalnie skonstruowanym przyrządzie. Wartości naprężenia obliczano, korzystając ze specjalnie opracowanego programu. Próbki pierścieniowe do badań przygotowywano według schematu: obróbka skrawaniem (toczenie i szlifowanie), hartowanie, odprężenie oraz selekcjonowanie próbek przez pomiar ich twardości – wykorzystano próbki o twardości HRC 56±2. Wybrane wyniki pomiaru naprężeń ostatecznych w warstwie wierzch-

niej pierścieni szlifowanych zewnętrznie zostały przedstawione w postaci zależności analitycznych i graficz-nych. Przedstawiono wpływ prędkości obwodowej ściernicy dla skojarzenia różnych wartości rzeczywistej głębokości szlifowania i posuwu. Przedstawiono także wpływ wartości stosunku v_c/v_w na przebieg i maksymalną wartość naprężeń ostatecznych.

The properties of the internal surfaces ground using CBN and Al$_2$O$_3$ grinding wheels

P. KOCHANIEWICZ, T. KARPIŃSKI

Koszalin University of Technology, ul. Racławicka 15/17, 75-620 Koszalin

The paper presents the results of the tests on surface microgeometry being formed during internal grinding by means of micro- and monocrystalline CBN and Al$_2$O$_3$ grinding wheels. Surface roughness was characterized by such parameters as: R_a, S, $r_{śr}$, Δ_a, KPS versus v_s, v_{fa}, v_w, a_e. They describe specific quality of internal grinding surfaces obtained due to work of each of grinding wheels. The detailed investigation proves that the best surfaces in respect of roughness and material ratio are obtained during the usage of the grinding wheel with microcrystalline CBN grain and at the smallest values of grinding power. Surfaces ground using the monocrystalline CBN grinding wheel are characterized by somewhat worse values of roughness, and their grinding demands greater power usage. The surface had the worst quality when Al$_2$O$_3$ grinding wheel was used. Roughness of these surfaces was completely different in quality from that achived while grinding with CBN grinding wheels. Moreover, the power of grinding in each case reached the largest value.

Keywords: *CBN and Al$_2$O$_3$ grinding wheels*, *surface roughness*, *internal surfaces grinding*

1. Introduction

The newest generation of the ceramic grinding wheels, including the grinding wheels from mono- and microcrystalline CBN grain, due to the best operating properties is considered to be extremely convenient to investigate the quality of the surfaces obtained, specifically compared to the conventional grinding wheels. It is supposed that perfect cutting qualities of the CBN grains and different character of cutting them [1, 4, 5, 6], compared to broadly used grains, should result in formation of the grinding surface of higher quality. This paper presents quantitative and qualitative description of this surface.

2. Methods of investigations

The investigations consisted in measurements of surface roughness and grinding power expressed by four different grinding parameters (v_s, v_{fa}, v_w, a_e). Each measurement was repeated 5 times. The programme assumed that all grinding wheels will be tested (Figure 1). The following roughness parameters were chosen as the dependent quantities: the height R_a, the horizontal S (ISO/DIN 4287), shape parameters as Δ_a (ISO/DIN 4287), $r_{śr}$ (mean radius of the local top of profile). In the

investigations, the measurement of the function represented by the curve of predicted point of the contact *PPC* was also carried out.

a)   *b)*   *c)*

Fig. 1. The grinding wheels used in investigations: a) Al_2O_3 grain, b) CBN with
microcrystalline 1B grain, c) CBN with monocrystalline 3B grain
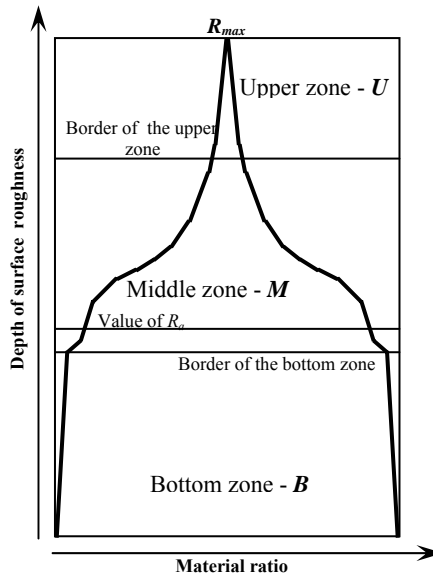
Fig. 2. The new idea of presentation of the material ratio curve

A new representation of material ratio curve is worthy of notice as the predicted point of contact curve is obtained in such a way that every section being a value approaches *a* for an adequate depth of roughness, spurts itself aside, symmetrically in relation to axis, which exceeds the value of 50% of material ratio (Figure 2). In the shape of figure (predicted point of contact curve – *PPC*), we can distinguish three zones. The upper zone *U* is characterized in such a way that the lines of the figure are very close one to another and they tend almost vertically to R_{max}. The bottom zone *B*, the distance between the lines of figure, approaches 100% of material ratio. And central zone *M* being included between zones *U* and *B*.

The bearing rings from the bearing steel ŁH 15 were used as samples, whose hardness was 64 ±2 HRC. The investigations were carried out on the grinder RUP 28 at the following processing parameters:

- wheel peripheral speed, v_s = 20; 27.5; 32.6; 35 m/s,
- speed of axial feed, v_{fa} = 0.5; 1; 1.34; 1.5 m/min,
- workpiece velocity, v_w = 40; 80; 160; 320 r.p.m.,
- depth of cut in one cross, a_e = 2; 2.5; 3.5; 4.5 μm.

It was assumed additionally that:

- roughing allowance, g_g = 0.08 mm , to pass
- number of crosses, i = 5.

The diagram of the experimental investigations was presented in Figure 3.
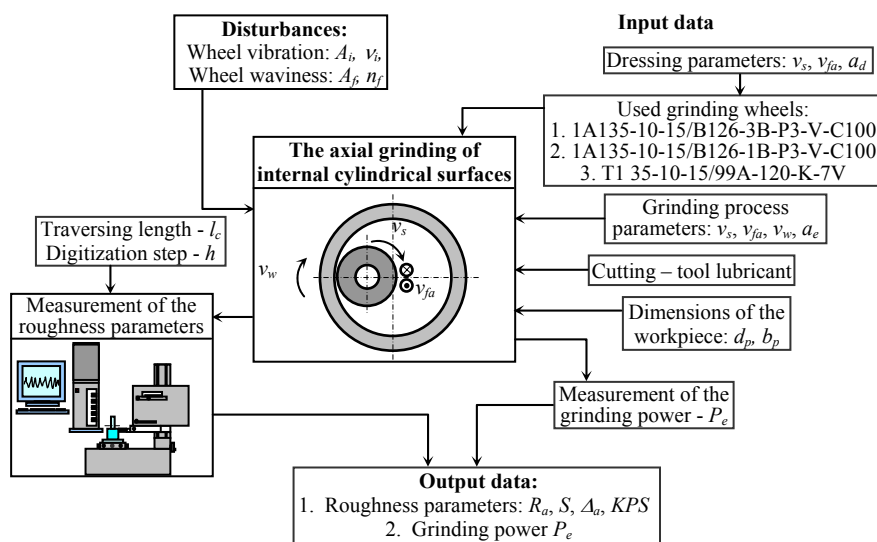
Fig. 3. The diagram of experimental investigations of internal grinding

The process of grinding of the bearing rings by the CBN grinding wheels was enhanced by the processing oil Polgrind 1A. In the case of grinding by the grinding wheel from Al$_2$O$_3$ grain, an aqueous solution of the oil Emulgol E-42 was applied.

3. Results of the experimental investigations

Analysis of the results of experimental investigations showed different features of the surfaces being ground by means of various wheels. From the curves presented in Figures 4 and 5 for CBN grinding wheel from microcrystalline grain it can be seen

that the parameters R_a and Δ_a achieve the smallest values, and $r_{śr}$, the largest. The surfaces are characterized by the highest material ratio at large value of the bottom zone B and small value of the middle zone M (Figures 6 and 7).
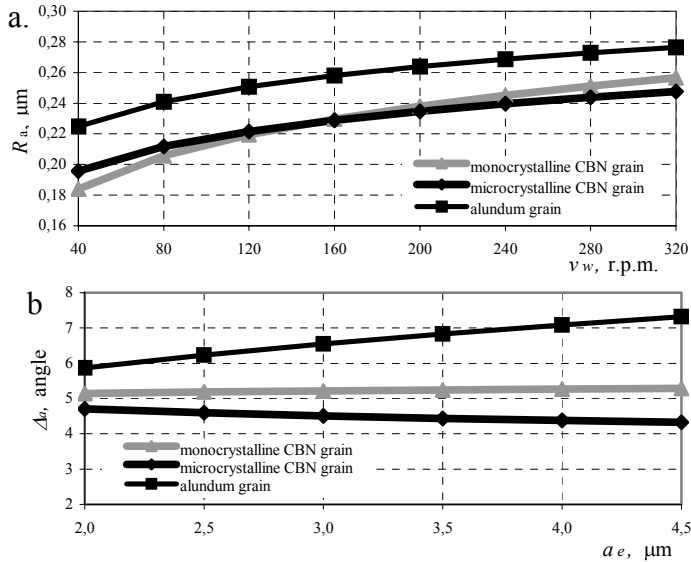
Fig. 4. The changes of roughness parameter: R_a (a) and Δ_a at changing parameters of grinding (b)
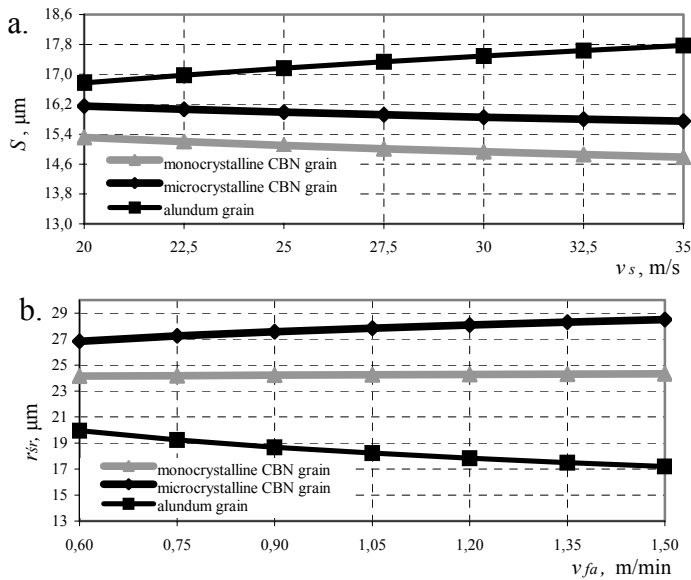
Fig. 5. The changes of roughness parameter: S (a) and $r_{śr}$ at changing parameters of grinding (b)
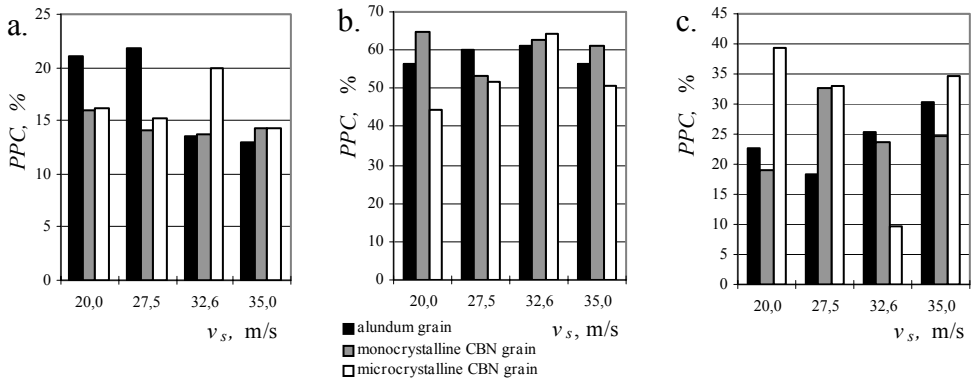
Fig. 6. The part of zones of the prognosed point of contact : a) upper, b) middle, c) bottom at changing wheel peripheral speed v_s, for the grinding process of the bearing rings surface
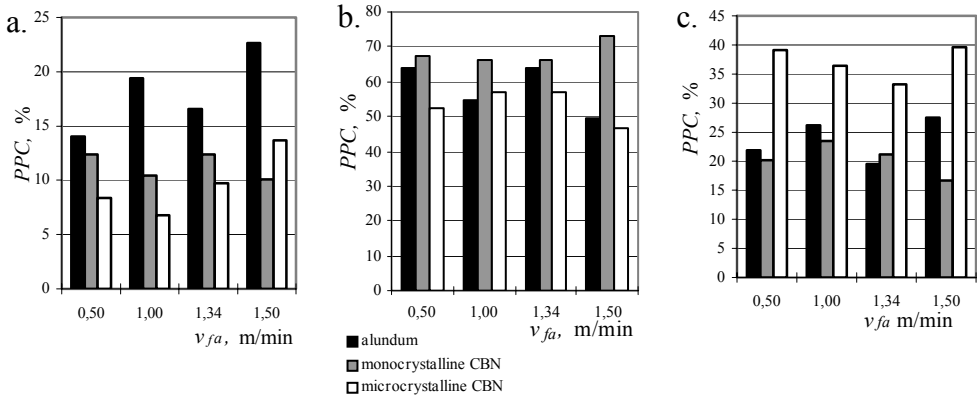
Fig. 7. The part of zones of the prognosed point of contact : a) upper, b) middle, c) bottom at changing speed of axial feed v_{fa}, for the grinding process of the bearing rings surface

The surfaces cut by means of the monocrystalline CBN grain are characterized, in comparison to these cut by microcrystalline CBN grain, by the larger value of the parameters R_a and Δ_a and the smaller values of the parameters S and $r_{śr}$. However, the values of parts of the bottom zone B are smaller, and the central zone M is larger from the values obtained after cutting the surfaces by means of the microcrystalline CBN grinding wheel. Therefore the material ratio of these surfaces is smaller. For the Al₂O₃ grinding wheel the parameters R_a, Δ_a and S reach the largest values, and $r_{śr}$, the smallest.

The material ratio of these surfaces is comparable to that obtained when a CBN wheel from monocrystalline grain is used, but the quality of their exploitation properties are decidedly the worst.

We dealt with the best properties of exploitation surface and simultaneously with the smallest power of grinding when CBN wheel from microcrystalline grain is used. This power is somewhat larger in the case of using the monocrystalline grains, and the largest – for Al_2O_3 wheel.

4. Summary

The investigations prove that the best surfaces in respect of roughness and material ratio are obtained due to usage of the grinding wheels with microcrystalline CBN grain, and the power of grinding reaches the smallest values. This is connected with the specific structure of the microcrystalline CBN grains as well as with their excellent physical and chemical properties [1–6]. Surfaces ground by means of the monocrystalline CBN grinding wheels are characterized by somewhat worse values of roughness, and their grinding requires larger power. This difference is associated with various structure of these monocrystalline grains, in comparison to the microcry-stalline ones. The surface had the worst quality when Al_2O_3 grinding wheels were used. Roughness of these surfaces totally differed in quality from that ground by CBN grinding wheels. At higher values of grinding parameters (v_s, a_e) it was possible to observe [3] burnings of surface as well. Moreover, the power of grinding in each case achives the largest values.

References

[1] Hamrol A., Konieczny R., Weiss Z.: *Badania procesu szlifowania otworów ściernicami z regularnego azotku boru*, Materiały XXI Naukowej Szkoły Obróbki Ściernej, Warszawa–Miedzeszyn, 1998.
[2] Karpiński T. et al.: *Sprawozdanie z wykonania projektu badawczego pt: „Badania w zakresie podstaw teoretycznych i doświadczalnych budowy narzędzi ściernych borazonowych”*, MEN, WSI, Koszalin, Wydział Mechaniczny, 1991.
[3] Kochaniewicz P.: *Kształtowanie mikrogeometrii wewnętrznych powierzchni walco-wych szlifowanych ściernicami z regularnego azotku boru*, praca doktorska, Wydział Mechaniczny Politechniki Koszalińskiej, Koszalin, 2000.
[4] Marciniak M.: *Proces szlifowania w ujęciu fenomenologicznym*, Prace Naukowe, Mechanika, z. 178, Politechnika Warszawska, 1999.
[5] Napierała J., Weiss Z.: *Właściwości warstwy wierzchniej po szlifowaniu ściernicami z regularnego azotku boru*, Materiały IV Konferencji Naukowo-Technicznej *Wpływ technologii na stan warstwy wierzchniej*, Gorzów Wielkopolski, 1985.
[6] Plichta J.: *Podstawy szlifowania ściernicami z mikrokrystalicznym ziarnem regularnego azotku boru ze spoiwem ceramicznym*, Monografie Wydziału Mechanicznego nr 58, Politechnika Koszalińska, 1996.

**Charakterystyczne właściwości powierzchni otworów
szlifowanych ściernicami CBN i Al$_2$O$_3$**

W pracy przedstawiono wyniki badań doświadczalnych nad kształtowaniem się mikro-geometrii powierzchni otworów walcowych, które szlifowano ściernicami z ziarnem mikro- i monokrystalicznego CBN oraz Al$_2$O$_3$. Mikrochropowatość powierzchni charakteryzowano za pomocą takich parametrów jak: R_a, S, $r_{śr}$, Δ_a, PPC w funkcji v_s, v_{fa}, v_w, a_e. Opisano charakterystyczne cechy powierzchni otrzymanych podczas szlifowania przez każdą z użytych ściernic. Dokonano również oceny jakościowej właściwości eksploatacyjnych tych powierzchni. Szczegółowe badania wykazały, że najlepsze powierzchnie zarówno pod względem chropowatości, jak i nośności uzyskuje się podczas szlifowania ściernicą z mikrokrystalicznym ziarnem CBN, a moc szlifowania osiąga najmniejsze wartości. Nieco gorszymi wartościami chropowatości charakteryzują się powierzchnie szlifowane ściernicą z monokrysta-licznym ziarnem CBN, natomiast sam proces szlifowania wymaga zwiększonej ilości energii. Chropowatość powierzchni szlifowanych ściernicą z ziarnem Al$_2$O$_3$ zdecydowanie odbiega od chropowatości powierzchni szlifowanych ściernicami CBN zarówno pod względem osiąganych wartości, jak i jakości powierzchni, a moc szlifowania w każdym przypadku osiąga największe wartości.

Thermal model of magnetic composites grinding process

B. KRUSZYŃSKI, J. PAZGIER

Łódź University of Technology, ul. Stefanowskiego 1/15, 90–924 Łódź, Poland

The main problem of grinding of magnetic composites is to combine high efficiency with low grinding temperature. This is difficult due to, among others, different properties of composite components. High temperature is dangerous especially for magnetic component whose integrity may be easily destroyed. To investigate grinding process of magnetic composites the thermal model was developed which enables calculation of temperature and temperature gradient distributions in the workpiece. Moving heat source of the triangular power density distribution of different parameters for each composite component was assumed. Different thermal properties of composite components were taken in consideration. The validity of the model was proved by the experiments where grinding temperatures were measured. An experimental stand, experimental results and some examples of calculations are presented in the paper. Crucial regions in the magnetic composite were found in which the highest temperature and temperature gradients occur and where surface integrity may be destroyed.

Keywords: *grinding, thermal model, magnetic composites*

1. Introduction

Grinding of composite materials is difficult, mainly due to different properties of composite components. It makes difficult to select optimal properties of grinding wheel and grinding conditions to satisfy quality requirements for all composite components.

Such a situation occurs in grinding "sandwich-like" magnetic composites (Figure 1) consisting of hard, brittle ceramic magnets of poor thermal conductivity and of soft, ductile metallic separators of good thermal conductivity and capacity. It creates entirely different conditions in creation of geometrical surface as well as in heat flow and thermal phenomena that occur under the surface for particular components of composite.

Machine components made of magnetic composites are widely used in typography. Such parts have to satisfy very high quality requirements for both surface roughness (usually R_a = 0.16–0.32 μm that requires grinding as finishing operation) and magnetic properties. The latter can easily be destroyed when high temperature is generated during grinding. Also, high temperature and high temperature gradients in grinding create conditions in which an integrity of magnetic component can be destroyed and cracking or chipping may occur.

All the problems mentioned above make selection of grinding parameters extremely difficult. To make it easier and more efficient the model of grinding process of magnetic

composite was developed in the Institute of Machine Tools and Production Engineering of Technical University of Łódź, Poland [1, 3]. The model enables calculations of heat fluxes, temperature and temperature gradient distributions in the sandwich-like composites on the basis of wheel and workpiece properties and grinding conditions. Also, it can be useful for scientific analysis of thermal effects in the composite materials and in optimisation of grinding conditions to produce high quality surfaces with high production rates.

2. The model

The construction of the sandwich-like magnetic composite is presented in Figure 1. Each magnetic part is separated from another one by a steel blade which ensures a proper strength of the whole composite as well as amplification of the magnetic flux. The dimensions (g_1, g_2 and H) of particular components of the composite may differ, depending on application.
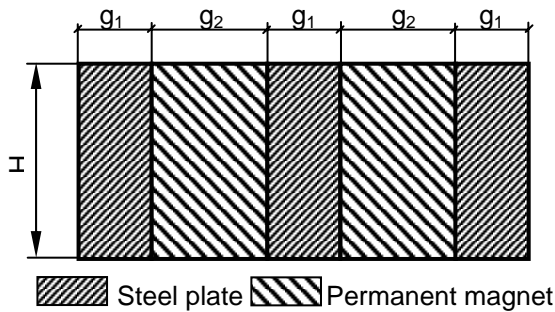
Fig. 1. Sandwich-like magnetic composite
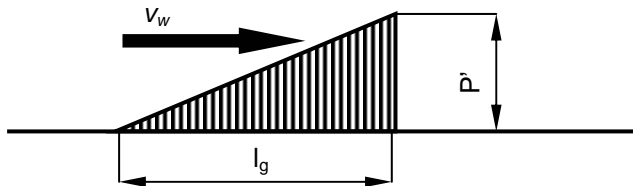
Fig. 2. The triangular power density distribution

The moving heat source of triangular power density distribution that represents thermal conditions at the wheel–workpiece interface was assumed, cf. Figure 2.

This is believed, e.g. [2, 5], that such a distribution approximates satisfactorily the actual thermal conditions in grinding.

Due to various configurations of wheel–workpiece contact lengths in relation to the composite elements widths the actual heat entering the workpiece distribution may be as complicated as it is shown in Figure 3 and may change during the grinding wheel movement along the workpiece surface. Also, another thermal conditions assumed in the model are shown in Figure 3.

A heat removal by convection from the upper surface being ground (excluding wheel–workpiece contact area) as well as from side and bottom surfaces of the composite was taken into consideration. Different convection coefficients ($C_1 = 20$ W/(m·K) and $C_2 = 6$ W/(m·K)) were assumed on different surfaces (Figure 3) due to differences in cooling conditions that may occur on these surfaces.
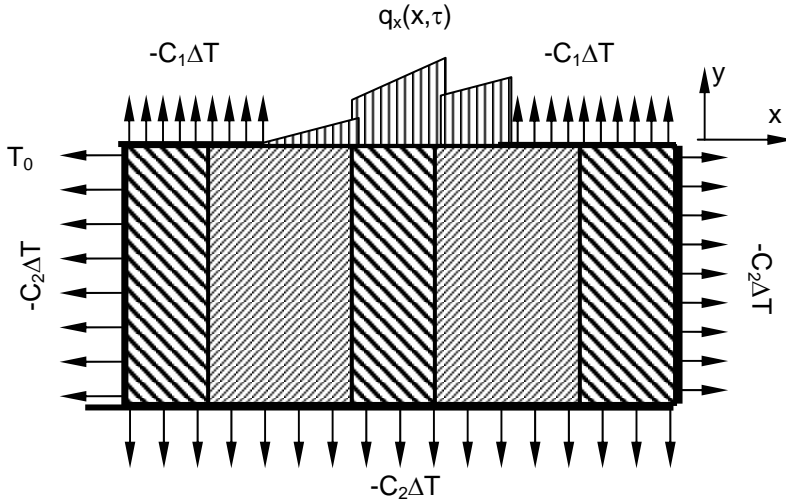
Fig. 3. Thermal conditions in grinding of magnetic composite assumed in the model

In order to calculate heat source parameters the following assumptions were accepted:
- the length of heat source is equal to a geometrical wheel–workpiece contact length l_g that can be calculated for surface grinding from the following equation:

$$l_g = \sqrt{a_e \, d_s} \, , \tag{1}$$

where a_e is an effective grinding depth and d_s is a grinding wheel diameter;
- all thermal properties are independent of temperature,
- heat source velocity is equal to the working speed v_w,
- energy partition ratio R can be calculated according to the wheel and workpiece materials configurations [4] from the following equation:

$$\frac{1}{R} = \left(\frac{\alpha_w \cdot v_s}{\alpha_g \cdot v_w} \right) \cdot \frac{\lambda_g}{\lambda_w} + 1 , \tag{2}$$

where: α_w, α_g, are thermal diffusivities of the workpiece and grinding wheel, respectively, λ_w, λ_g are thermal conductivities of the workpiece and grinding wheel, respectively, v_s is wheel speed and v_w is working speed.

To calculate the temperature distribution in the work material the following, well-known differential Fourier–Kirchoff equation is to be solved:

$$\frac{\partial T}{\partial \tau} = \alpha_w \left(\frac{\partial^2 T}{\partial x^2} + \frac{\partial^2 T}{\partial y^2} + \frac{\partial^2 T}{\partial z^2} \right) + \frac{\dot{q}_V}{\rho_w c_{pw}} = \alpha_w \nabla^2 T + \frac{\dot{q}_V}{\rho_w c_{pw}} , \tag{3}$$

where: T is temperature, τ is time, α_w is thermal diffusivity, ρ_w is specific weight, c_{pw} is specific heat, q_v is a rate of local internal energy per unit volume, and x, y, z are coordinates.

Due to the complex heat source density distribution the finite-element method (FEM) was applied to solve Equation (3) and to find temperature and temperature gradient distributions in the composite. Because the most important temperature changes were expected to be close to the surface being ground, the non-uniform elements dimensions (Figure 4) were applied in vertical direction to enable precise analysis of the temperature distribution in this region. It allows prediction of the temperature with the higher accuracy in the near-surface region.
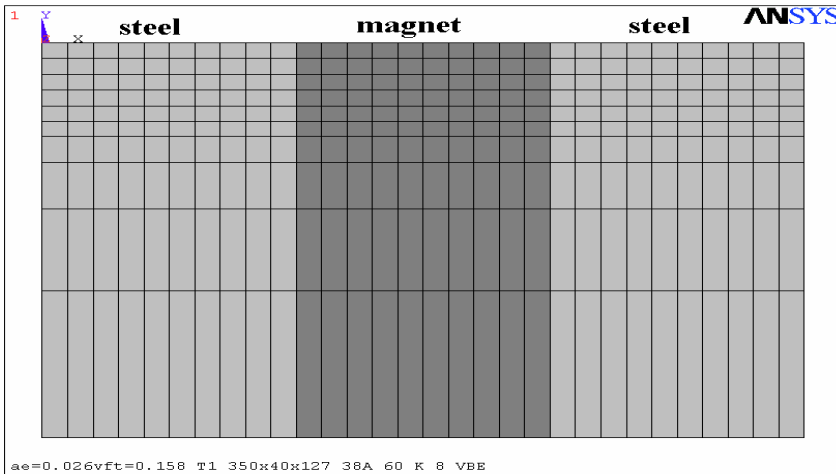
Fig. 4. The division of the magnetic composite into elements for FEM calculation

3. Model verification

Total grinding power was calculated as a product of the tangential grinding force F_t and the wheel speed v_s. The maximum power density P'_{max} of the triangular heat source at wheel–workpiece interface was then calculated as:

$$P'_{max} = \frac{RP}{2l_g b_D} = \frac{RF_t v_s}{2l_g b_D},$$

(4)

where: P is total grinding power; R is energy partition ratio, cf. Eq. (2); b_D is grinding width. To measure tangential grinding force an experimental stand shown in Figure 5 was developed.
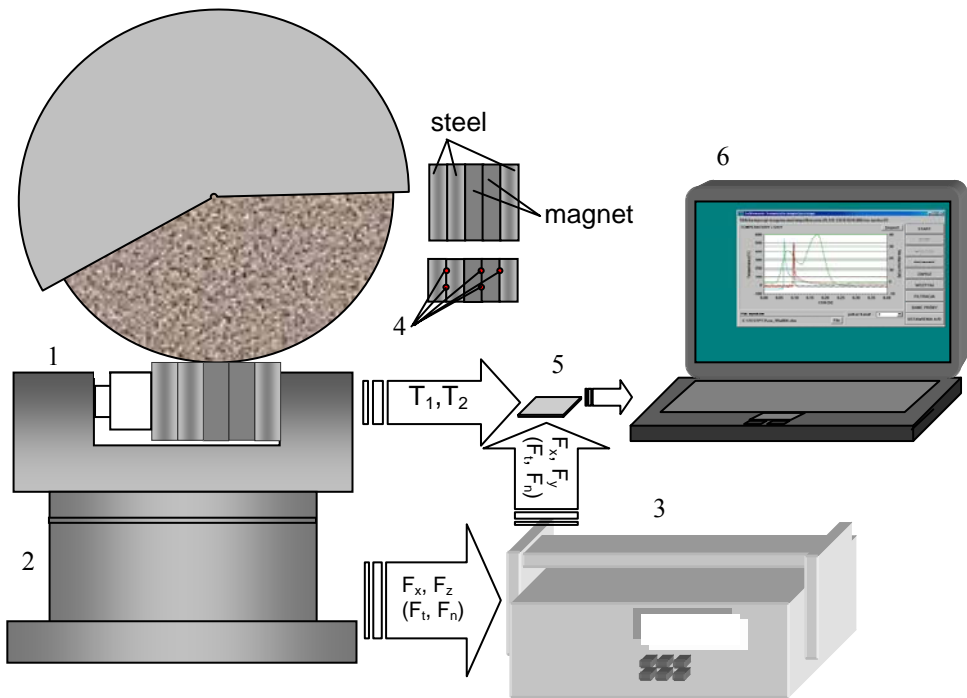
Fig. 5. Experimental stand setup

Special vise (1) mounted on a Kistler 9072 dynamometer (2) with a Kistler 4019 amplifier (3) was connected to an AC/DC card placed in a PC computer. A special computer program was developed to control measurement procedure as well as to record and process the measurement results. The stand also enables measurements of grinding temperature in selected points of magnetic composite by means of thermocouples (4).

The results of temperature measurements were compared with computing results to verify the validity of the model.

Experiments were carried out in the following conditions:

- grinding wheel: T1 350×63×127 25A 80 G 12 VBEP,
- wheel speed v_s = 26 m/s,
- working speed v_{ft} = 0.1–0.5 m/s,
- depth of cut a_e = 0.005–0.050 mm,
- fluid, emulsion.

On the basis of the measurements the following equations for calculating grinding forces were derived:

$$F_t = 33 + 54 \cdot a_e - 27 \cdot v_{ft} \quad \text{(for magnet)}, \tag{5}$$

$$F_t = 60 + 498 \cdot a_e - 53 \cdot v_{ft} \quad \text{(for steel)}. \tag{6}$$

The forces calculated on the basis of these equations were then applied to calculate heat source power density distribution, cf. Equation (3).

Table 1. Properties of the materials used in the magnetic composite

Material property	Steel (1.0530)	Magnet (BaFe$_2$O$_3$)
Thermal conductivity λ [W/(m·K)]	100	0.8
Specific heat c [J/(kg·K)]	460	800
Material density ρ [kg/m^3]	7840	4240

Table 2. The comparison of the results being measured and calculated

Cutting conditions	Temperature during grinding of magnetic composites [°C]					
	Measured			Calculated		
	1	2	3	1	2	3
a_e = 0.032 mm, v_{ft} = 0.16 m/s	790	750	500	775	731	496
a_e = 0.036 mm, v_{ft} = 0.24 m/s	890	830	550	860	812	486
a_e = 0.029 mm, v_{ft} = 0.25 m/s	589	559	400	580	570	370
a_e = 0.012 mm, v_{ft} = 0.28 m/s	560	539	370	540	520	330

FEM calculations of temperature and temperature gradients were done for the materials that constitute magnetic composite. Properties of these materials are presented in Table 1.

The comparison of the results being measured and calculated (Table 2) shows that accuracy of the calculations is satisfactory. The differences between calculations and measurements are, in the most cases, well below 10% of the values being measured. The differences are caused mainly by simplifications taken in the model.

4. Calculation results

Temperature was calculated for some characteristic points of the composite (see Figure 6) for a configuration in which two steel plates were separated from each other by a magnetic part: in the middle of steel plates (points 1, 2 and 10), in the middle of the magnet (point 6) and in both elements close to steel–magnet interfaces (points 3, 4, 5, 7, 8 and 9). The results of calculations of surface temperature at these points are shown in Figure 7.
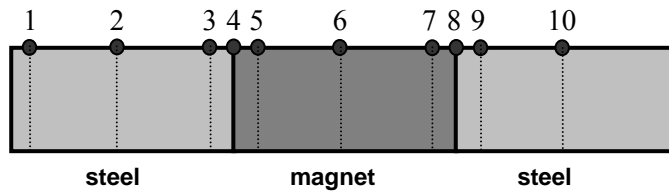
Fig. 6. Points selected to carry out temperature calculations
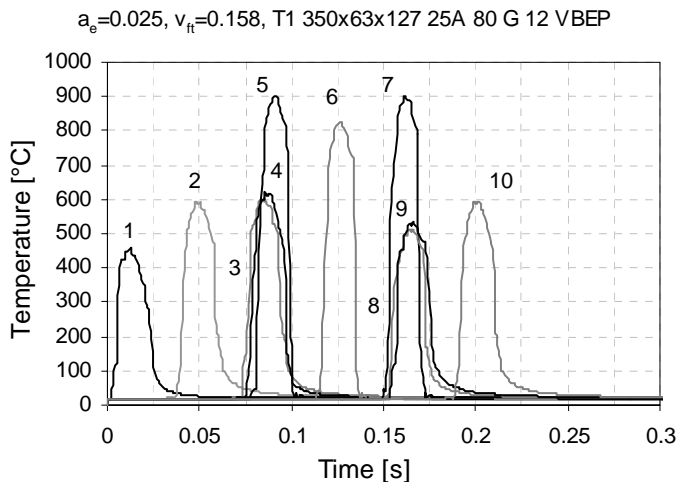
Fig. 7. Results of calculations of temperature distribution in
magnetic composite at selected points

It can be seen from this figure that the grinding temperature at the surface strongly depends on the material being ground. The maximum temperature for steel ranges from 450 ºC to 600 ºC depending of the point considered. For magnetic parts it changes from 820 ºC to 900 ºC. This is due to different heat distribution and different thermal properties of these materials. The power density is higher when grinding steel due to higher grinding forces, but much better thermal conductivity of this material makes grinding temperatures lower than that obtained for magnetic ceramics.

The maximum temperature depends also on the distance from the steel–magnet contact surface. For example, the higher temperature in points 5 and 7 than that in point 6 results from an additional heat flux flowing from the steel plate to the magnetic component. The temperature at point 1 is influenced by a heat removal from a side surface by convection.
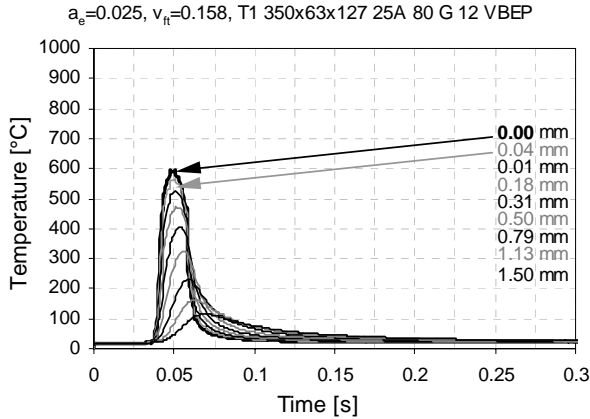
Fig. 8. Results of calculations of temperature distribution in a steel
part of magnetic composite (point 2 in Figure 5)

Also a distribution of the temperature with a depth below the surface strongly depends on the material being ground. Good thermal conductivity of steel enables heat transfer to a deeper layers of materials and elevated temperatures are observed even at a depth of 1.5 mm (see Figure 8).
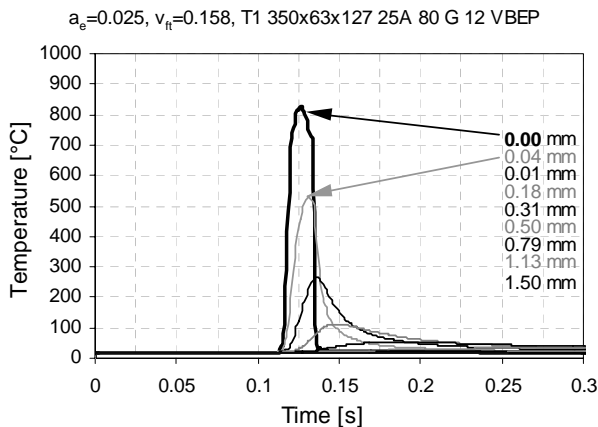
Fig. 9. Results of calculations of temperature distribution in a magnetic
part of magnetic composite (point 6 in Figure 5)

The temperature distribution for magnetic part of the composite (see Figure 9) shows very shallow penetration of heat in this material caused by its very poor thermal conductivity, over 100 times lower than thermal conductivity of steel (see Table 1). Changes of temperature are hardly observed in the layers deeper than 0.2 mm under the surface.

The temperature distribution in the neighbourhood of the steel–magnet interface is shown in Figure 10. It confirms the above statement that conditions of heat penetration in steel are entirely different from those in magnet. It can also be seen from Figure 10 that magnetic part is additionally heated at the steel–magnet interface, which creates specific isotherms pattern in the corner of the magnetic component and very high thermal loading in this region, different from that observed in the remaining part of this component.

Such a thermal loading of magnetic component poses a danger of loosing magnetic properties (when grinding temperature exceeds the Curie point, which approaches 450 ºC in this case) not only in the near-surface region but also in the neighbourhood of the steel–magnet interface. It also indicates that very high temperature gradient distribution may be observed especially in the sub-surface region and in the corners of magnetic component.

To examine it in more detail the calculations of the temperature gradient were also carried out and their results are presented in Figure 11. This figure shows that temperature gradient in magnetic component, in the grinding conditions applied, is as high as 12631 ºC/mm and close to that of the surface being ground. This creates high thermal stresses which may destroy integrity of the material. Also the stresses at the steel–magnet interface caused by uneven thermal elongation of these materials can cause a serious cracking of brittle magnetic ceramic.
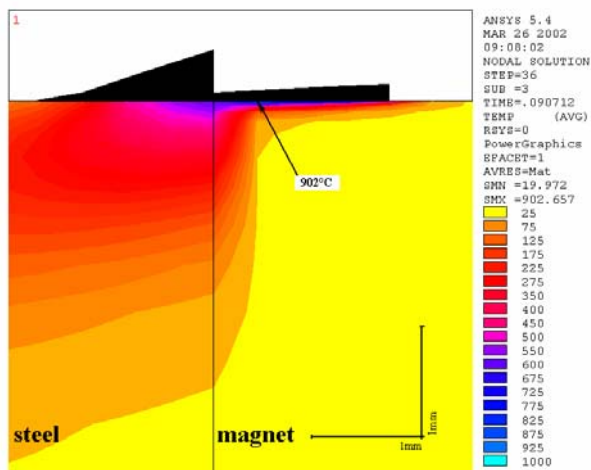
Fig. 10. An example of temperature distribution in the magnet composite
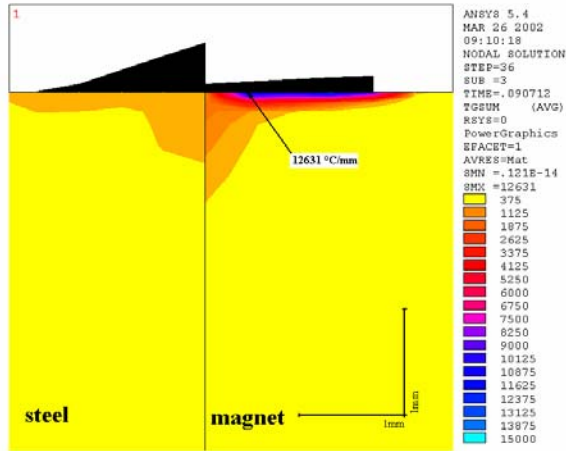
Fig. 11. An example of thermal gradient distribution in the magnet composite

It also was found that on the border between steel and magnetic parts of the composite a strong barrier to heat flow in a horizontal direction occurs. It results in even higher temperature and thermal gradient just in the corner of the magnetic material and thermal conditions at this part of composite may be a crucial criterion for the selection of process parameters [3].

5. Concluding remarks

- Thermal model developed enables calculations of temperature and temperature gradient distributions in the sandwich-like magnetic composites,
- The validity of the model was confirmed experimentally.
- The calculations carried out showed different temperature distribution and temperature penetration in different parts of the composite.
- The uneven temperature distribution may cause such a detrimental effects as a loose of magnetic properties or cracking and chipping of magnetic material.
- The model may be useful for prediction of temperature and thermal stresses in composite materials as well as for selection and/or optimization of grinding parameters.

References

[1] Kruszyński B., Pazgier J.: *Temperatures and forces in grinding of magnetic composites DMC 2000*, Kosice, pp. PL65–PL67.
[2] Malkin S., Anderson R.B.: *Thermal aspects of grinding. Part I. Energy partition,* Journal of Engineering for Industry, No. 11, 1974, pp. 1177–1183.
[3] Pazgier J.: *Optymalizacja procesu szlifowania kompozytu magnetycznego*, PhD thesis, Politechnika Łódzka, Łódź, 2001.

[4] Rowe W.B. et al.: *Avoidance of thermal damage in grinding and prediction of damage threshold*, Annals of the CIRP, 37(1), 1988, pp. 327–330.

[5] Vansavenant E.A.: *Subsurface integrity model in grinding*, PhD thesis, K.U. Lueven, 1987.

Model cieplny procesu szlifowania kompozytów magnetycznych

Głównym problemem w szlifowaniu kompozytów magnetycznych jest trudność w uzyskaniu wysokiej wydajności obróbki i utrzymanie niskiej temperatury szlifowania. Sprawia to trudności z powodu różnych właściwości poszczególnych składników kompozytu. Wysokie temperatury szlifowania mogą być niebezpieczne szczególnie dla składnika magnetycznego kompozytu, którego integralność łatwo zniszczyć. Aby badać proces szlifowania kompozytu magnetycznego, opracowano cieplny model tego procesu, który umożliwia obliczanie rozkładu temperatury i gradientu temperatury w obrabianym przedmiocie. Założono źródło ciepła o trójkątnym rozkładzie gęstości mocy i o parametrach różniących się dla poszczególnych składników kompozytu. Różne właściwości cieplne składników kompozytu były również wzięte pod uwagę. Poprawność opracowanego modelu została sprawdzona podczas badań eksperymentalnych, w których mierzono temperaturę szlifowania. W artykule opisano stanowisko do badań doświadczalnych, wyniki badań oraz przykładowe wyniki obliczeń. Znaleziono obszary kompozytu magnetycznego, w których występuje najwyższa temperatura obróbki oraz najwyższy gradient temperatury.

Information about PhD thesis at the Civil Engineering Faculty and the Mechanical Engineering Faculty of the Wrocław University of Technology

Title: ***Bearing capacity of subsoil in the case of closed plasticity conditions*** **(in Polish)**
Nośność graniczna podłoża w przypadku zamkniętych warunków plastyczności

Author: Andrzej Batog
Supervisor: Professor Ryszard J. Izbicki
Promoting Council: Council of the Civil Engineering Faculty
Reviewers:
    Doctor Elżbieta Stilger-Szydło, Professor of WUT
    Doctor Antoni Florkiewicz, Professor of PUT

Abstract: The paper deals with the application of closed plasticity conditions in the solution of the capacity problems of the subsoil loaded with direct foundations. Its main thesis is as follows: the introduction of closed plasticity conditions to solutions of the limit equilibrum theory (for the rigid-plastic body model) allows one to obtain results that describe the field of the subsoil deformation close to that observed in reality (the occurrence of both effects of soil dilatation and contraction) as well as to make allowance for the conditions of soil consolidation and partly the influence of geological history on soil capacity.

The paper introduces and discusses new forms of the linear, closed plasticity condition with the asymmetrical surface of plasticity. The influence of the preconsolidation pressure on different soils, from weak and compressible to strongly preconsolidated, was analysed. The primary anisotropy was considered. It was connected with natural sedimentation and consolidation under the tension conditions close to the conditions of oedometric test. The presented forms of the plasticity surfaces referred to the combination of boundary surfaces experimentally identified by Hvorslev and Roscoe.

The methods of the estimation of lower and upper bounds of the bearing capacity in the case of the subsoil loaded with direct foundation were presented for plane-strain conditions and axisymmetry. The values of exact bearing capacity were determined using the method of characteristics.

The paper shows and discusses a series of important practical relations referring to the influence of the preconsolidation pressure on the dilatation and contraction effects in the loaded subsoil manifested itself in static and kinematics solutions. The results obtained were verified by more advanced calculations for an elasto-plastic body model.

Title: *Computer analysis of prefabricated building in WWP system in the area of mining damage* (in Polish)
Analiza komputerowa budynku wielkopłytowego systemu WWP na terenach szkód górniczych

Author: Jacek Paweł Barański
Supervisor: Professor Jeremi M. Sieczkowski
Promoting Council: Building Engineering Faculty of the Wrocław University of Technology
Reviewers:
    Professor Gustaw Rakowski, Warsaw University of Technology
    Professor Zbigniew Zembaty, Technical University of Opole
Date of PhD thesis presentation: July 5th, 2000
Ph.D. work is available in Main Library and Scientific Information Centre of WUT
The paper contains: 77 pages, 78 figs, bibliography, 40 items
Keywords: *paraseismic quakes, prefabricated building, computer modelling, FEM analysis, horizontal joint*

Abstract: Prefabricated concrete buildings are very popular in Poland. Most of them were built in years 1960-1980. Diagnosing their technical state, possibilities of strengthening and safety of use become indispensable and concerns the state of construction and breakdown hazard. Computer techniques become suitable tools together with specialized software for static–strength analysis. In many situations, we can model complex structure systems in such an arrangement that permits us to foresee the effects of mining activity on an object at any loading combination.

Special attention was paid to twelve-storey buildings with prefabricated elements' horizontal joints. They have a decisive influence on buildings behaviour during dynamic events. Paraseis-mic quakes are dangerous especially for this of type of buildings and can be the reason of pre-failure states. Besides mechanical defects they can shorten the working life of buildings. Because the above joints could not be investigated in natural scale in laboratory, computer techniques of modelling was used. They allowed a sufficiently exact analysis of internal forces and displacements in construction of a building. FEM LUSAS programme with spectral response method was used. They influence of paraseismic quakes on prefabricated buildings was investigated, and especially bad technical condition of horizontal joints was considered. Change in the value of spring stiffness made possible passing from fixed connections (monolithic) to hinges and to imitate, with good approximation, damage of joints. Dynamic calculations of buildings, which were strengthened, allowed us to assess their resistance to paraseismic quakes.

Title: *Influence of rheologic properties of bituminous mixtures on pavement deformation* **(in Polish)**
Wpływ właściwości reologicznych mieszanek mineralno-asfaltowych na deformacje nawierzchni drogowych

Author: Piotr Mackiewicz
Supervisor: Professor Antoni Szydło
Promoting Council: Building Engineering Faculty of the Wrocław University of Technology
Reviewers:
    Professor Wojciech Grabowski, Poznań University of Technology
    Professor Bogdan Stypułkowski, Wrocław University of Technology
Date of PhD thesis presentation: April 25th, 2001
Ph.D. work is available in Main Library and Scientific Information Centre of WUT
The paper contains: 160 pages, 214 figs, bibliography, 281 items
Keywords: *rutting test, rheological parameters, viscoelastic models*

Abstract: A model for investigation of bituminous mixtures in the rutting test was described. The model was based on FEM. The properties of bituminous mixtures in this model were described by rheological parameters specific to linear viscoelastic models of Maxwell, Zerner and Burgers. Identification of the rheological parameters was carried out in the creep test in the third cycle of loading. The smallest error of approximation of parameters' identification was found for Burgers' model and the biggest for Zerner's model. The depth of ruts was calculated using the model described and the rheological parameters found. Next, the depth of ruts was compared with the depth of ruts determined in the rutting tester. It has been found that the models of Burgers and Maxwell are in good agreement with the results of rutting tester. Maxwell's model including small number of parameters is appropriate for practical purposes. It has been observed that the efficiency of rut forecasting is reliable when rheological parameters are determined in the third cycle of loading at the temperature of 50 ºC and at the loading of 0.1–0.5 MPa. Moreover, it has been shown that 1400 s time of loading in the creep test may be reliable for identification of parameters. For this time, it has been observed the that creep established correlates with the rutting established. On the grounds of this correlation, relation between depth of rut in the rutting tester and deformation in the creep test was determined. Furthermore, an empirical relation between the depth of rut, mixture content and number of loading cycles was described. Analysis of the results enabled us to determine the most important rheological parameters of the mixture and the factors acting on formation of ruts, such as: temperature, time and value of loading. There is a considerable susceptibility of bituminous mixture to rutting, depending on viscosity coefficient in Maxwell's model and Burgers' model and delayed elasticity module in Burgers' model. Using the rheological parameters, viscoelastic model of pavement was proposed. Based on of this model it is possible to forecast depth of ruts in different climatic conditions and periods of exploitation.

Title: *Capacity of elements of public transport network* **(in Polish)**
         Przepustowość elementów sieci komunikacji zbiorowej

Author: Maciej Kruszyna
Supervisor: Professor Antoni Szydło
Promoting Council: Council of Institute of Civil Engineering
Reviewers:
   Professor Andrzej Rudnicki, Kraków University of Technology
   Professor Paweł Śniady, Wrocław University of Technology
Date of PhD thesis presentation: December 15th, 1999
Ph.D. work is available in Main Library and Scientific Information Centre of WUT
The paper contains: 106 pages, 38 figs, bibliography, 128 items
Keywords: *traffic, analyse, traffic model, town public transport*

Abstract: The dissertation deals with the capacity of elements of public transport network. It takes into consideration the specificity of traffic of public transport vehicles on a separated way shared by buses and trams. It is assumed that a section of way closed at both ends by light-controlled junctions is a characteristic and representative element of transport network. The analysis is focused on maximal capacity which may be achieved when the parameters of traffic have an optimal structure. Using field experiments the range of changes in parameters of traffic was analysed, while using models – the influence of the mentioned range of changes on the capacity was estimated. Two models of traffic were constructed for the analysed element of the network: the deterministic and the stochastic models.

Information about habilitations at the Civil Engineering Faculty and the Mechanical Engineering Faculty of the Wrocław University of Technology

Title: *Random vibration problems of the plate-type constructions supporting machines* **(in Polish)**
Problemy losowych drgań płytowych konstrukcji wsporczych pod maszyny

Author: Władysław Mironowicz
Promoting Council: Council of Faculty of Civil Engineering
Reviewers:
    Professor Tadeusz Chmielewski, Technical University of Opole
    Professor Janusz Kawecki, Kraków University of Technology
Date of habilitation colloquium: May 28th, 1999
Habilitation monograph is available in Main and Scientific Information Centre of the Wrocław University of Technology
The monograph contains: 101 pages, 33 figs, bibliography, 128 items
Keywords: *supporting structure, plate, dynamics, random parameters, random load*

Title: *Initiating and critical stresses versus stress failure in compressed concrete* **(in Polish)**
Naprężenia inicjujące i krytyczne a destrukcja naprężeniowa w betonie ściskanym

Author: Jerzy Hoła
Promoting Council: Civil Engineering Faculty of the Wrocław University of Technology
Reviewers:
    Professor Kazimierz Furtak, Kraków University of Technology
    Professor Mieczysław Kamieński, Wrocław University of Technology
    Professor Jerzy Ranachowski, Warsaw University of Technology
Date of habilitation colloquium: April 17th, 2000
Habilitation monograph is available in Main Library and Scientific Information Centre of the Wrocław University of Technology
The monograph contains: 182 pages, 106 figs, bibliography, 294 items
Keywords: *compressed concrete, stress failure, initiating stresses, critical stresses, acoustic investigation methods*

Title: ***Time couplings incorporated in organizational methods of complex construction* (in Polish)**
Sprzężenia czasowe w metodach organizacji złożonych procesów budowlanych

Author: Zdzisław Hejducki
Promoting Council: Civil Engineering Faculty of the Wrocław University of Technology
Reviewers:
    Professor Zbigniew Błochwiak, Kraków University of Technology
    Professor Kazimierz Jaworski, Warsaw University of Technology
    Professor Kazimierz Czapliński, Wrocław University of Technology
Date of habilitation colloquium: January 10th, 2001
Habilitation monograph is available in Main Library and Scientific Information Centre of the Wrocław University of Technology
The monograph contains: 126 pages, 32 figs, bibliography, 111 items
Keywords: *time couplings, construction work, organizational methods*

Title: ***Deflections of the reinforced concrete beams being sustainedly loaded. Comparison study* (in Polish)**
Ugięcia długotrwale obciążonych belek żelbetowych. Studium porównawcze

Author: Mariusz Szechiński
Promoting Council: Board of the Civil Engineering Faculty of the Wrocław University of Technology
Reviewers:
    Professor Jan Biliszczuk, Wrocław University of Technology
    Professor Tadeusz Ćwirko-Godycki, Gdańsk University of Technology
    Professor Władysław Kuczyński, Technical University of Łódź
Date of habilitation colloquium: September 13th, 2000
Habilitation monograph is available in Main Library and Scientific Information Centre of the Wrocław University of Technology
The monograph contains: 244 pages, 112 figs, bibliography, 288 items
Keywords: *reinforced concrete, beams, sustained loads, deflections*

Title: ***Interaction of Environmental Thermal Radiation
on the Building* (in Polish)**
***Oddziaływanie cieplnego promieniowania środowiska zewnętrznego
na budynek***

Author: Henryk Nowak
Promoting Council: Wrocław University of Technology, Faculty of Civil Engineering
Reviewers:
    Professor Piotr Klemm, Technical University of Łódź
    Professor Wojciech Marks, Polish Academy of Science, Piaseczno
    Professor Lech Śliwowski, Wrocław University of Technology
Date of habilitation colloquium: Juni 2nd, 1999
Habilitation monograph is available in Main Library and Scientific Information Centre of the Wrocław University of Technology
The monograph contains: 196 pages, 78 figs, bibliography, 196 items
Keywords: *a building, environment, longwave radiation, modelling*

Information for Authors